Geological characterisation of the Bamboesberg Member within the Molteno-Indwe coalfield, Eastern Cape Province, South Africa.

Submitted as partial requirement for the degree

MSc Geology

Submitted to:

Department of Geology

Faculty of Natural and Agricultural Sciences

University of Pretoria

Submitted by:

Mzoli Breakfast

21832162

Date of Final Version: 05 February 2024

ABSTRACT:

The Bamboesberg Member forms the basal member of the Late Triassic Molteno Formation. It hosts the two economically significant coal seams in the Molteno-Indwe coalfield, namely the Guba and Indwe seams. The Molteno-Indwe coalfield is located mainly in the northern region of the Eastern Cape Province in South Africa.

The Council for Geoscience (CGS) drilled thirteen vertical boreholes within the Molteno-Indwe coalfield between 1984 and 1986. These cores were retrieved from the National Borehole Core Depository in order to characterise the sandstones of the Bamboesberg Member. To achieve this objective, the cores were logged in detail and scanned using a hyperspectral imaging scanner. Additionally, sandstone samples were collected for physio-chemical analysis.

The Bamboesberg Member consists of fining-upwards cycles of sandstones, interbedded with argillaceous units and, in certain areas, coal. The coal seams typically occur on top of the argillaceous successions. These sandstones are classified as sub-litharenite and are sourced from the recycled orogenic provenance. Through SEM-EDX analysis it was observed that the sandstones contain large euhedral detrital garnets and sub-rounded zircons.

The coal samples from the Bamboesberg Member were assessed for their rare earth element potential. Most samples displayed a rare earth element concentration ranging from 100 to 200 ppm, while five samples exhibited a higher concentration of over 350 ppm. The minerals hosting the rare earth element were observed to be monazite, parisite, and xenotime.

Three-dimensional (3D) modelling revealed that the Bamboesberg Member has a concave shape at its centre and the maximum thickness observed is 120 meters. It tapers off to the north, pinching out to 20 m north of Aliwal North. The Bamboesberg Member is more exposed in the western and central parts of the Molteno-Indwe coalfield. Consequently, the western and central portions of the coalfield have potential for further coal prospecting within the Molteno-Indwe coalfield.

KEYWORDS:

Bamboesberg Member; Molteno-Indwe coalfield; provenance; mineral dominant map; rare earth elements; 3D modelling

DECLARATION:

I, **Mzoli Breakfast,** declare that the thesis/ dissertation, which I hereby submit for the degree MSc at the University of Pretoria, is my own work and has not previously been submitted by me for a degree at this or any other tertiary institution. I, the undersigned, furthermore declare that:

- I understand what plagiarism is and am aware of the University's policy in this regard.
- I declare that this assignment (e.g. essay, report, project, assignment, dissertation, thesis, etc.) is my own original work. Where other people's work has been used (either from a printed source, Internet or any other source), this has been properly acknowledged and referenced in accordance with Departmental requirements.
- I have not used work previously produced by another student or any other person to hand in as my own.
- I have not allowed, and will not allow, anyone to copy my work with the intention of passing it off as his or her own work.
- I understand the Department of Geology's policy on plagiarism and the criteria set for using Turnitin by the Department.
- I acknowledge that I am allowed to use Turnitin to evaluate my own work prior to submission.

Full names:	Mzoli Breakfast
Student number:	21832162
Date submitted:	
Degree:	M.Sc. in Geology
Topic of work:	Geological characterisation of the Bamboesberg Member within the Molteno-Indwe coalfield, Eastern Cape Province, South Africa.
Supervisor(s):	Prof. Nils Lenhardt, Department of Geology, University of Pretoria
Co-supervisor(s):	Prof. John Hancox, Evolutionary Studies Institute, University of the Witwatersrand
Signature:	

DEDICATION:

I dedicate my thesis to my son, Ndalo Breakfast and my late mother, Sisiyena Blakfesi, who was my rock.

ACKNOWLEDGEMENTS:

ACADEMIC OUTCOMES

Conference proceedings:

<u>M Breakfast</u>, AO Kenan, LS Kirstein, T Mothupi, (2021). Potential for rare earth elements in the Molteno-Indwe coalfield, Eastern Cape Province. (Council for Geoscience Conference 2021).

<u>M Breakfast</u>, AO Kenan, N Lenhardt, J Hancox (2023). Basin analysis of the Molteno-Indwe coalfield. Eastern Cape Province, South Africa (Geocongress Conference at Stellenbosch, 2023).

<u>M Breakfast</u>, AO Kenan, N Lenhardt, J Hancox (2023). Geological characterization of the Bamboesberg Member within the Molteno-Indwe coalfield, Eastern Cape Province, South Africa. (Council for Geoscience Quarter Technical Workshops).

TABLE OF CONTENTS

LIST OF FIGURES

LIST OF TABLES

LIST OF ABBREVIATIONS

ARANZ   Applied Research Association of New Zealand

BSE   Back-scattered electron

CGS   Council for Geoscience

CIA   Chemical index alteration

EC   Eastern Cape

ESI   Evolutionary Studies Institute

EDX   Energy dispersive X-ray analysis

GPS   Global Positioning System

HREE   Heavy rare earth elements

ICPMS   Inductively coupled plasma mass spectrometry

IUPAC   International Union of Pure and Applied Chemistry

IRP   Integrated Resource Plan

KZN   KwaZulu-Natal

L.O.I.   Loss on ignition

LREE   Light rare earth elements

LWIR   Long-wave infrared light

NBCD   National Borehole Core Depository

PPM   Parts per million

REE   Rare earth element

RGB   Red, Green and Blue

SABS   South African Bureau of Standards

SACS   South Africa Committee for Stratigraphy

SEM   Scanning electronic Microscope

SEM-EDX   Scanning electronic Microscope-energy dispersive X-ray analysis

SRTM   Shuttle Radar Topographic Mission

SWIR   Short-wave infrared light

XRF   X-ray fluorescence spectrometer

1 Introduction

1.1 Background

There are 19 generally accepted coalfields in South Africa (Figure 1), covering an area of about 9.7 million hectares (ha) (Hancox and Götz, 2014). The distinction among these coalfields is based on geographical factors and differences in the mode of sedimentation, origin, formation, distribution, and consistency of coal qualities. South African coalfields occur within three intervals of geologic time: the Early Permian (Artinskian-Kungurian) Ecca Group (Vryheid Formation), the Middle-Late Permian (Ufimian-Kazanian) Beaufort Group, and the Late Triassic (Carnian) Molteno Formation within the Stormberg Group (Hancox, 2019; Hancox and Götz, 2014). With the exception of coal from the Late Triassic Molteno Formation, all coal in the main Karoo Basin occurs in the distal sector on a stable platform overlying the Kaapvaal Craton.

The Molteno-Indwe coalfield is located within the Molteno Formation of the Stormberg Group. The coalfield, resembling the shape of a horseshoe, spans an area of approximately 4,400 km2 and the most part of the coalfield is located in the northern part of the Eastern Cape. It also extends into the Free State and KwaZulu-Natal (KZN) provinces. This coalfield has a long and intricate history of mining activity. Coal mining operations began in 1864 on the Cyphergat farm near the town of Molteno. By 1877, multiple mines were also operating near the town of Indwe. The coal from the Molteno-Indwe coalfield was primarily extracted to supply energy to the newly discovered diamond mines in Kimberley (Prévost, 2013).

The discovery of gold in the Witwatersrand in 1886 stimulated further exploration of coal, which led to the discovery of a higher-quality coals in the Witbank coalfield in Mpumalanga Province and the Vryheid coalfield in KZN Province, respectively. These new discoveries resulted in a decrease in coal production in the Molteno-Indwe coalfield, and eventually the production ceased altogether (Cobban et al., 2009).
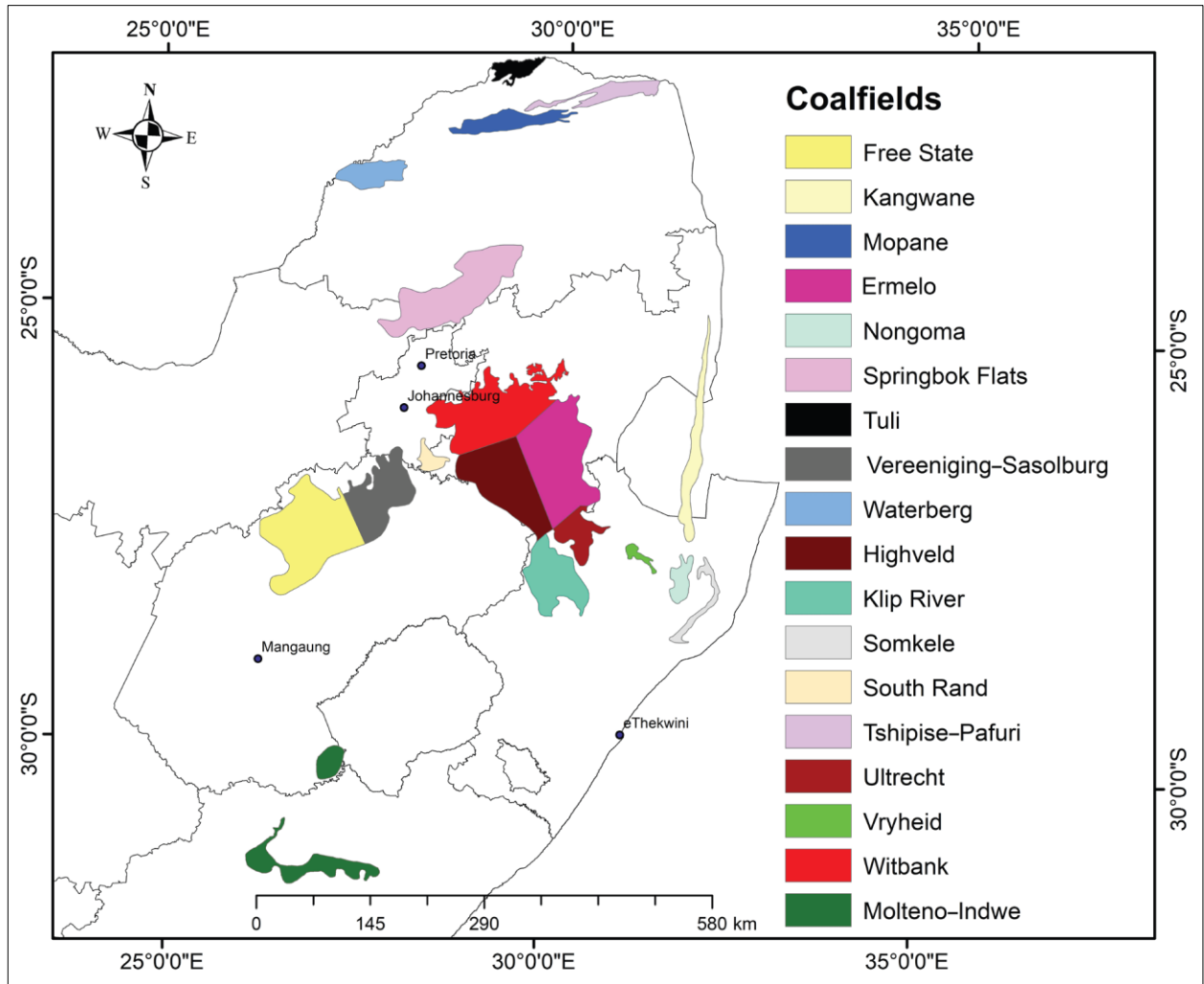
Figure 1. Nineteen coalfields of South Africa (Data from the Council for Geoscience Data Portal (https: https://www.geoscience.org.za/cgs/systems/data-management-portal/)).

1.2 Rationale for undertaking research

The Molteno-Indwe coalfield has been the subject of previous work, which focused mainly on stratigraphy and the coals of the Molteno Formation, with a particular emphasis on the Indwe and Guba seams. The Indwe Member is the only member that has been submitted and accepted by South Africa Committee for Stratigraphy (SACS) 1980 within the coalfield.

Several research topics have been covered in the coalfield, including Turner's (1975) comprehensive regional studies of the stratigraphy and geological history of the Molteno Formation. Christie (1981) investigated the stratigraphy and sedimentology of the Molteno Formation, while Heinemann (1988) focused on the macroscopic and chemical characteristics of the Guba seam. Most studies on coal geology in the Molteno Formation involved rank determination, resource estimation, and ultimate analysis, with coal deposits being irregularly distributed within small, isolated areas.

J.M. Anderson and H.M. Anderson conducted a comprehensive palaeoecological and palaeontological investigation, which included a detailed sedimentological investigation. Furthermore, they collected a large number of fossil plants and insects from the Molteno Formation, amassing a collection of over 30000 catalogued slabs from 100 plant and insect assemblages from 69 localities (areas up to 1 km diameter) which are currently housed at the Evolutionary Studies Institute (ESI) in Johannesburg, South Africa. Much scientific research has emerged from the catalogue. The fossil plants have been described in several monographs and papers (Anderson & Anderson 1983, 1989, 1993a; Scott, et al., 2004) and Reik (1974, 1976) described the associated insect fauna. The sedimentological setting of the biota has been investigated by Cairncross et al. (1995) and Anderson et al. (1998).

Hancox (1998) integrated stratigraphical, sedimentological, and palaeontological studies of the Burgersdorp Formation and lowermost Molteno Formation.

A comprehensive geological characterisation of Molteno Formation members is crucial, especially for the Bamboesberg Member, which is the basal member of the Molteno Formation. The geological characterisation aims to improve the existing geoscientific understanding of the provenance, deposition environment and sedimentary facies of the Bamboesberg Member. Due to the limited availability and increasing demand for rare earth elements, coal has been identified as a source of these valuable metals. It is vital to assess the concentration of rare earth elements in the coal seams of the Bamboesberg Member. This study comes after the CGS conducted a coal assessment investigation within the coalfield in 2018-2019. CGS's study (2020) revealed that the Molteno-Indwe coalfield coal seams (that is, the Guba and Indwe coal seams) have the potential to generate electricity through the use of small-scale modular power plants. In addition, these coal seams could be combined with biomass, which is abundant in the area, to generate electricity.

1.3   Aims of this project

The primary objectives of this study are multifaceted, encompassing several key research aspects within the Bamboesberg Member. The study aims to achieve a comprehensive classification and detailed characterisation of the sandstones present in the Bamboesberg Member. This involves examining their composition, texture, sedimentary features, and other relevant attributes to gain a thorough understanding of their geological properties.

Additionally, the study focuses on evaluating the potential of REE within the coal seams found in this specific member. This assessment is crucial as it provides valuable insights into the presence and concentration of REE within the coal, which can be helpful for potential extraction of these critical elements from coal ash.

To enhance the understanding of the geometrical architecture of the Bamboesberg Member, a 3D geological modelling technique is employed.

1.4 Study Area

The study area occurs within the Molteno-Indwe coalfield, which covers approximately 4 400 km^2 in areal extent, mainly in the northern part of the Eastern Cape Province, but also extending into the south of the Free State Province. The coalfield forms a horseshoe-shaped belt extending south-westwards from Aliwal North to Burgersdorp, Jamestown, Molteno, and Sterkstroom; then west-east from Dordrecht, lndwe, the Guba area and Cala; and north-eastwards toward Elliot, Gubenxa, Engcobo, and Maclear areas (Figure 2).
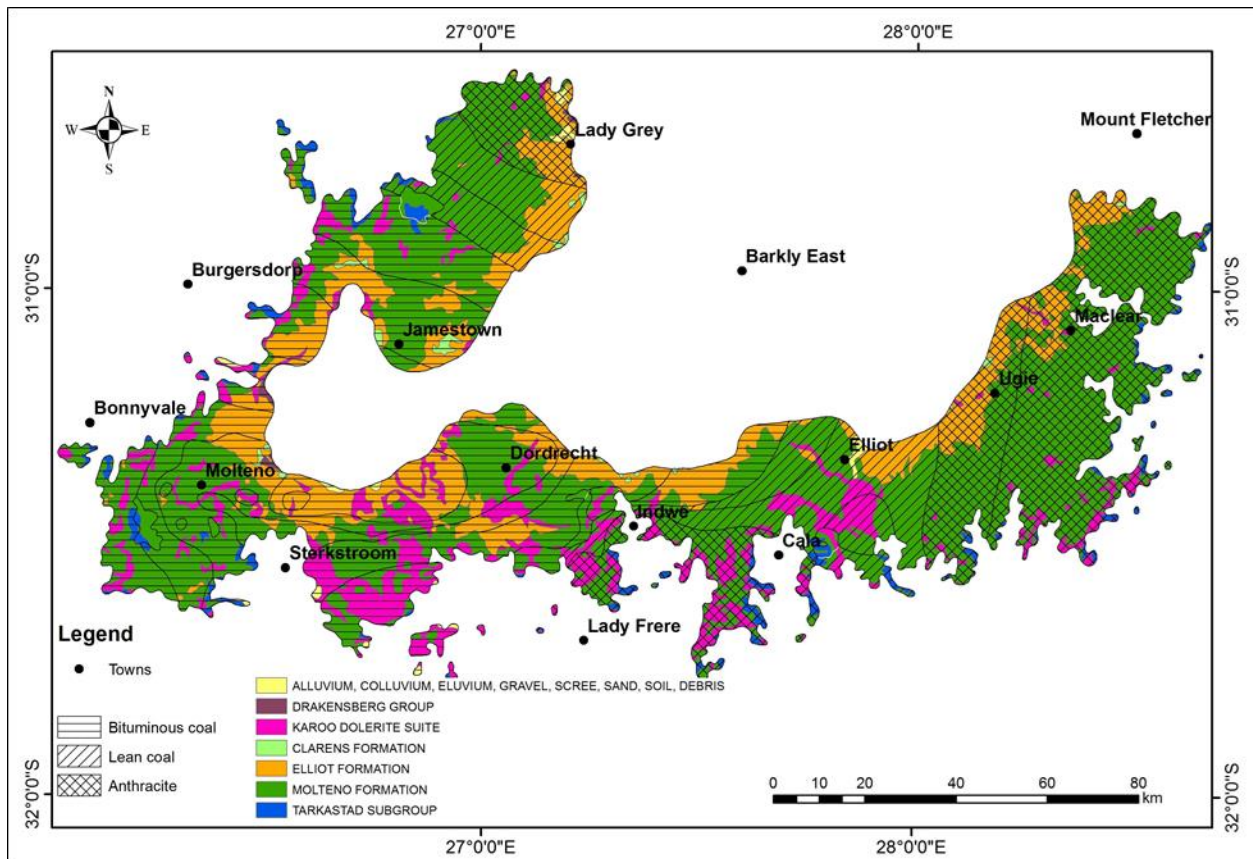
Figure 2. Geological map of Molteno-Indwe coalfield (Data from the Council for Geoscience Data Portal (https: https://www.geoscience.org.za/cgs/systems/data-management-portal/)).

2 Regional Geological Setting

2.1 Background

The main Karoo Basin is generally interpreted as a retroforeland basin that formed adjacent to the Cape Fold Belt (Johnson, 1996; Catuneanu et al., 1998; Catuneanu et al., 2001). The basin developed through the influence of subduction, compression, collision, and terrane accretion along the southern margin of Gondwana. The primary subsidence was regulated by flexural (supralithospheric) and dynamic (sublithospheric) loading, which also created space to accommodate sedimentary fill within the Karoo Basin (Viglietti, 2016; Hancox et al., 2019). The primary process of subsidence in the main Karoo Basin was based on orogenic loading, with flexural tectonics subdividing the basin into three flexural provinces (Figure 4): the foredeep, forebulge, and backbulge (Catuneanu, 2004; Catuneanu et al., 2005). The location of the forebulge and foredeep changed due to orogenic loading and unloading events in the Cape Fold Belt (Viglietti, 2016). Late Carboniferous (320 Ma) to Middle Triassic (247.2 Ma and 237 Ma) sediments filled these flexural provinces of the main Karoo Basin (Catuneanu et al., 1998; Catuneanu et al., 2001; Johnson, 1996). The deposition of sediments was later replaced by the intrusion of a large igneous province that formed dolerite dykes and sills (183 Ma). In the Middle Jurassic (174.1 to 163.5 Ma), the basaltic lava of the Drakensberg Group capped the main Karoo Basin (Chima et al., 2018).

The main Karoo Basin covers almost 70% of South Africa and the whole of Lesotho, with subsidiary extensional basins in southern African countries such as Namibia, Botswana, Swaziland, Zimbabwe, Zambia, and Mozambique as per Figure 3 below. (Veevers et al.,1994; Johnson, 1996; Hancox, 2019).
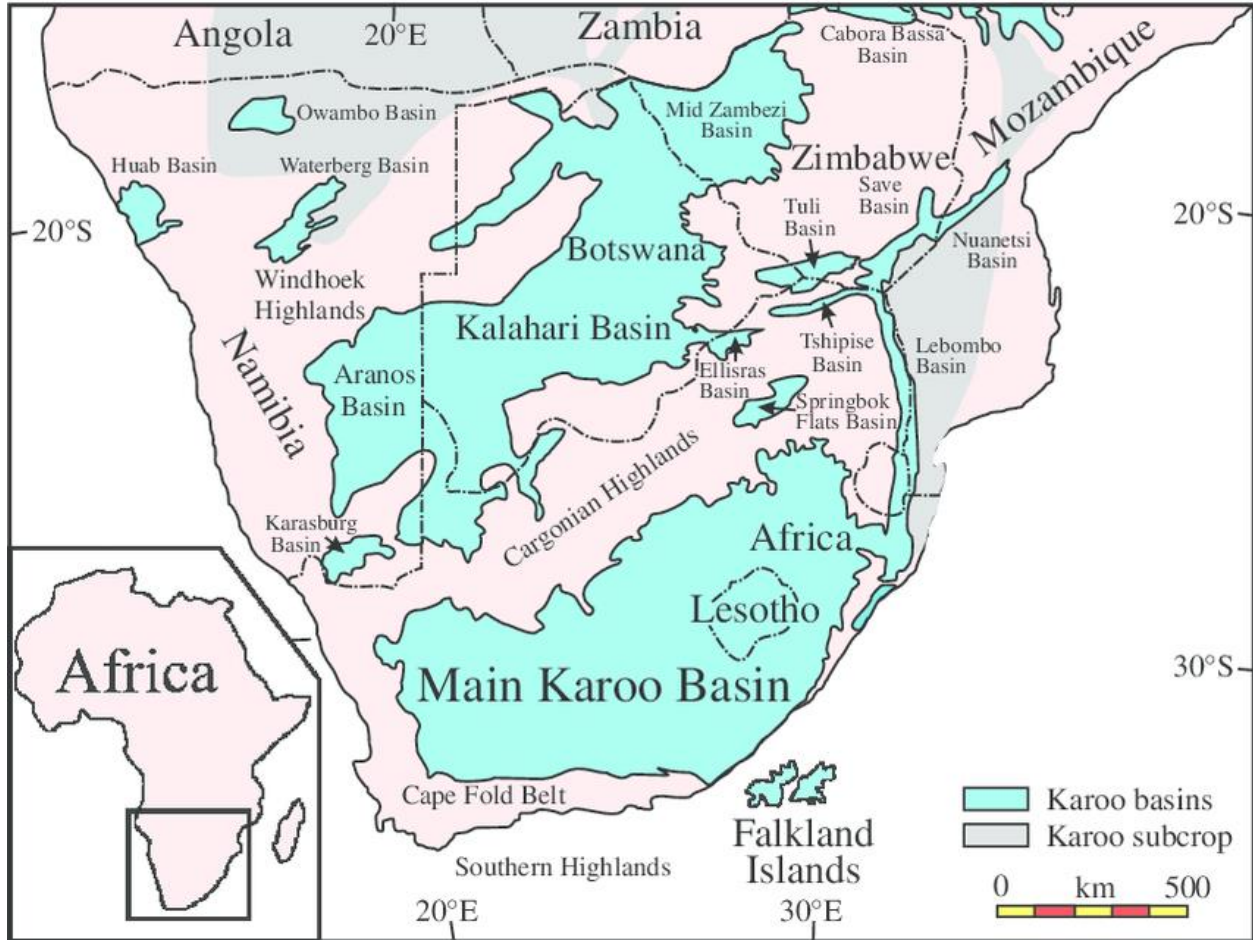
Figure 3. The distribution of the Karoo basins (from Catuneanu et al., 2005). The pre-breakup position of the Falkland Islands is that of Veevers et al. (1994).
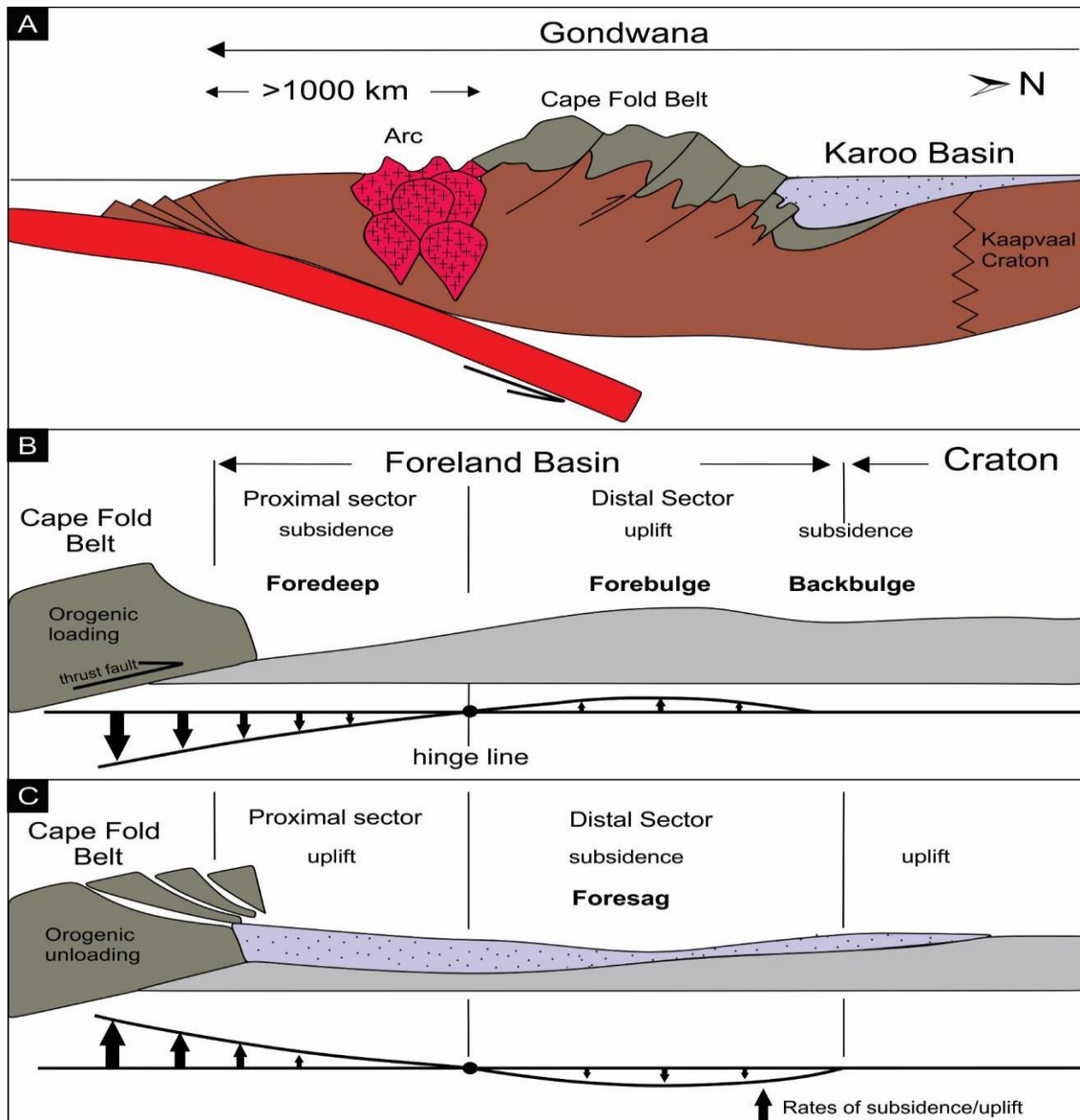
Figure 4. Tectonic setting and evolution of the Karoo retro-arc foreland basin Illustrating: (A) The subduction of the Palaeo-Pacific plate underneath the Gondwana plate. (B) Orogenic loading event of the Cape Fold Belt, generating the different flexural drop zones (i.e., foredeep and forebulge) within the foreland basin. (C) Orogenic unloading which generated the uplift and erosion of the Cape Fold Belt and the development of the foresag in the distal sector in which reworked sediments deposited (Adapted from Catuneanu et al., (1998)).

2.2 Main Karoo Basin Stratigraphy

The main Karoo Basin comprises four main sedimentary lithostratigraphic subdivisions, namely the Dwyka, Ecca, Beaufort, and Stormberg groups, capped by the Drakensberg basalts of the Middle Jurassic. The Dwyka Group, which consists of glacial deposits, is found at the bottom, followed by the Ecca Group, which consists of marine sediments. This group, in turn, is overlain by the Beaufort Group, which primarily consists of deltaic deposits. The Beaufort Group is overlain by fluvial and aeolian deposits of the Stormberg Group (Figure 5) (Veevers et al., 1994; Johnson, 1996; Bordy et al., 2005a; Catuneanu et al., 2005). The entire Karoo Supergroup is intruded by dolerites (dykes and sills) and capped by the basaltic rocks of the Drakensberg Group (Veevers et al., 1994).

The glaciogenic Dwyka Group is deposited paraconformably on the Witteberg Group of the Cape Supergroup and overlain by the Prince Albert Formation of the Ecca Group (Catuneanu et al., 2005). The Ecca Group sediments accumulated during the Permian epoch between the Cisuralian to Lopingian (Catuneanu et al., 2005). The Beaufort Group, overlying the Ecca Group. The deposition of the Beaufort Group occurred during the Late Permian, specifically in the Lopingian age, and extended into the Middle Triassic period (Bordy et al., 2004a; Catuneanu et al., 2005). The Late Triassic to Early Jurassic Stormberg Group rests unconformably on the Beaufort Group and consists of the Molteno, Elliot, and Clarens Formations that are capped by the Drakensburg Group (Turner, 1975; Hancox, 1998; Bordy et al., 2004).
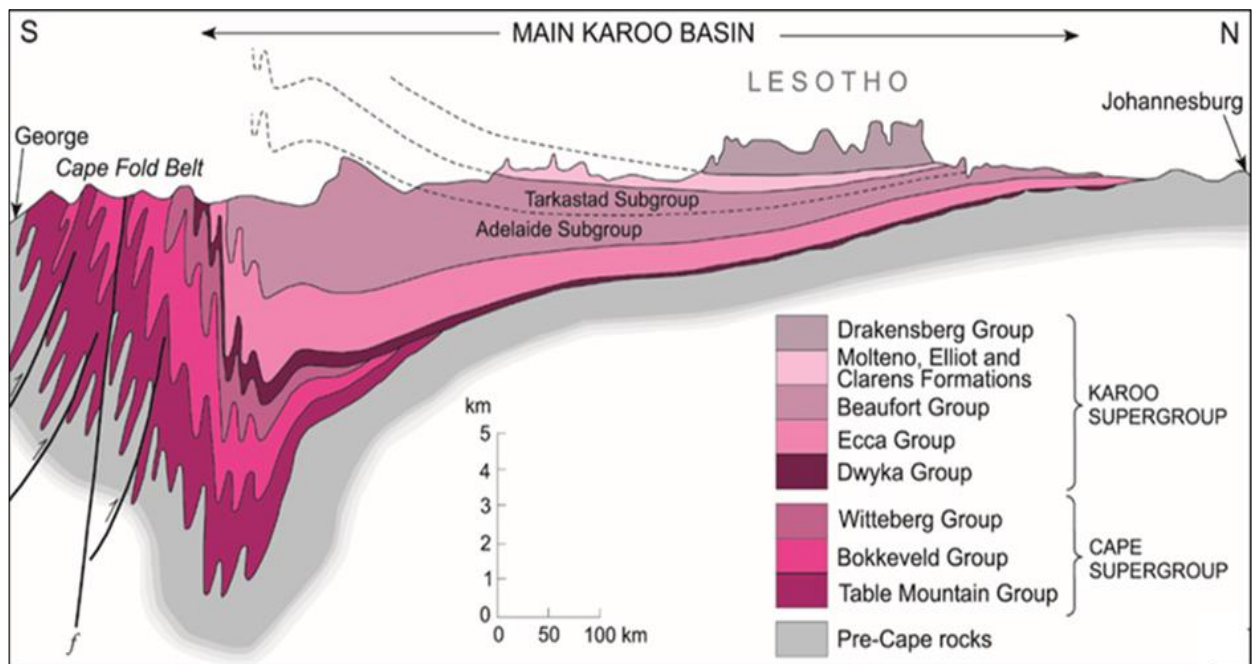
Figure 5. Schematic south-north section across the main Karoo Basin and Cape Fold Belt. (Johnson et al., 2006).

2.2.1 Dwyka Group

The Late Carboniferous and Early Permian glacial Dwyka sediments form the base of the main Karoo Basin. The Dwyka Group uncomfortably overlies the Cape Fold Belt (Witteberg Group) in the southern basin, whereas it conformably overlies the Namaqua-Natal Belt (Bushmanland) and the Msikaba Formation in the south (Catuneanu et al., 1998; Baiyegunhi, 2015). Within the main Karoo Basin, the Dwyka Group is represented by clastic rocks such as diamictites and fluvio-glacial sandstones, indicating a glacial environment. Its maximum thickness is approximately 800 m (Bangert et al., 1999; Herbert and Compton, 2007).

2.2.2 Ecca Group

Ecca sediments represent the marine transgression across the main Karoo Basin and diachronously overlie the Dwyka Group (Catuneanu et al., 2005; Phillips et al., 2014; Baiyegunhi et al., 2017). The Ecca Group generally consists of clastic sedimentary rocks such as mudstone, siltstone, sandstone, conglomerate, and coal seams within the Early Permian Vryheid Formation (Cadle et al., 1993; Catuneanu et al., 2005; Nyathi, 2014.). The Pietermaritzburg, Vryheid, and Volksrust Formations are stratigraphical subdivisions of the Ecca Group and occur in the northern part of the main Karoo Basin. In the southern part of the main Karoo Basin, the Ecca Group consists of five formations: 1) the Prince Albert, 2) Whitehill, 3) Collingham, 4) Rippon-, and 5) Fort Brown Formations (Uys, 2007).

2.2.3 Beaufort Group

The Beaufort Group sediments are the thickest and most extensive within the main Karoo Basin, reaching a thickness of more than 3 km (Bordy and Catuneanu, 2002). It overlies the Ecca Group deposited by fluvial-deposits of the Permo-Triassic (Turner, 1981). The Beaufort sediments resulted from the uplift of the Cape Fold Belt. These sediments migrated diagonally northward through the rivers that flowed through the bottom of the former salty to the freshwater basin, along a 500 km long piedmont slope, to the westward sloping line of sediment transport (Johnson et al., 1997; Nyathi 2014) In addition, Bamford (2004) noted that the Beaufort Group deposits indicate braided rivers and meandering streams developed in the region as the region's climate dried up and basins filled with sediment from the Cape-Fold Belt.

The Beaufort Group is divided into two subgroups: Adelaide and Tarkastad subgroups (SACS, 1980). The Adelaide Subgroup forms the base of Beaufort Group, comprising greenish- grey and grayish-red mudstone and fine-grained sandstone and it is overlain by the Tarkastad Subgroup, which comprises more sandstone and red mudstone (Johnson et al., 1997; Cartesio et al., 2017).

The Adelaide Subgroup is subdivided into Koonap, Middleton, and Balfour Formations. The lowermost Koonap Formation comprises greenish silty-mudstones and sandstones in a fining-upward sequence deposited when a high-energy braided river system graded into a lower-energy meandering river system. The Middleton Formation comprises of dark red and green-grey mudstones interbedded with sandstones in an overall fining upward sequence (Turner, 1981; Catuneanu et al., 1998)

The Balfour Formation is subdivided into the Palingkloof, Elandsberg, Barberskrans, Daggaboersnek, and Oudeberg members. The Balfour Formation has a pronounced lithological variation that is characterised by alternating sandstone and mudstone (Nyathi 2014).

The Tarkastad Subgroup of the Beaufort Group restricted to the eastern half of the main Karoo Basin consists of the Katberg and Burgersdorp Formations. The Katberg Formation is predominantly arenaceous in nature with minor thin (2–10 m), red and greenish grey mudstones. The Burgersdorp Formation, which is predominantly argillaceous rocks, is overlain by the Molteno Formation of the Stormberg Group (Turner, 1981; Catuneanu et al., 2005; Gastaldo et al., 2013; Hancox and Götz, 2014).

2.2.4 Stormberg Group

The sedimentary succession of the Stormberg Group deposited within the foresag is subdivided into fluvio-lacustrine Molteno, Elliot, and Clarens Formations (Figure 6) capped by volcanic rocks of the Drakensberg Group (Turner, 1975; Christie, 1981; Bordy, et al., 2005a; Catuneanu et al., 2005). Considering that the study succession occurs within the Molteno Formation, only a comprehensive overview of the Molteno Formation has been provided. The Formation is overlain by the Elliot Formation, which consists of a solid red or purplish colouration of mudstone and minor sandstone that is often coarse at the base and is very persistent and calcareous (Bordy et al., 2005b; Catuneanu et al., 2005; Cobban et al., 2009). The Elliot Formation is topped by the youngest sedimentary rocks of the Clarens Formation, which consists of white, cream or in places pink fine-grained sandstone and thin/silty sandstone beds (Bordy et al., 2004; Bordy and Catuneanu, 2002). The Drakensberg Group, which consists mostly of basaltic lava, minor tuff, and agglomerate, caps the sedimentary succession of the main Karoo Basin (Bordy et al., 2005a).
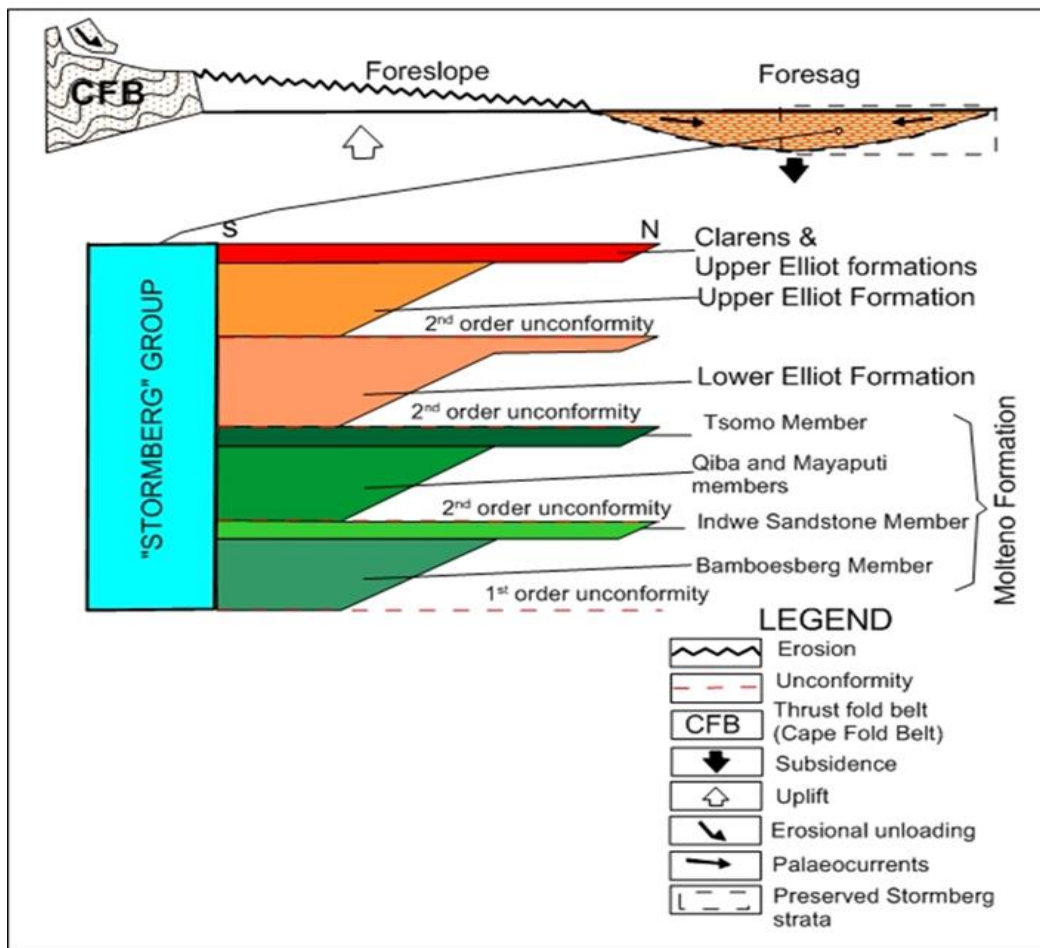
Figure 6. Generalised stratigraphic distribution and tectonic setting for the Stormberg Group (Bordy et al., 2005).

2.3 Stratigraphy of the Molteno Formation

The Molteno Formation is considered to have been deposited by an integrated braided river system and consists of conglomerates, sandstone, mudstone, and coal seams (Rust, 1962; Turner, 1975, 1971; Christie, 1981; Hancox, 1998). The formation attains a maximum thickness of approximately 625 m in the south between Indwe and Maclear and thins northwards to less than 10 m around Bethlehem and Harrismith (Christie, 1981; MacDonald, 1993; Bordy et al., 2005b). The Molteno Formation consists of several members. At the bottom of the Molteno Formation is the Bamboesberg Member comprising fining upwards cyclothems, which are capped by the sheet-like coarse sandstone of the Indwe Member (Christie, 1981; Hancox and Rubidge 2023). The Indwe Member is overlain by the upper members of the Molteno Formation. Various authors (Turner, 1975, 1975; Christie, 1981; MacDonald, 1993) partitioned the upper members into various members, whereas Hancox (1998) referred to the upper members as transitional members. Bordy et al., (2005a) combined the upper members into one informal unit that they referred to as Tsqima succession. In this study, the stratigraphic nomenclature given is that of Christie (1981). It must be mentioned that only the Indwe Member has been officially submitted and accepted by the South Africa Committee for Stratigraphy (SACS).

Table 1. Various authors divided the upper Molteno Formation into different members (as shown in the table below).

Turner (1975, 1977)	Christie (1981)	MacDonald (1993)	Hancox (1988)	Bordy et al. (2005)
Tsomo Member	Loskop Member	Tsomo Member	Transitional Members	Tsqima succession
	Tsomo Member			
Rose Glen Member	Qiba Member	Qiba Member		
Mayiputi Member	Mayiputi Member	Mayiputi Member		

2.3.1 Bamboesberg Member

In the southern central of the main Karoo Basin, the Bamboesberg Member is sandwiched between the Burgersdorp Formation (Beaufort Group) and the Indwe Member of the Molteno Formation (Hancox and Rubidge 2022). The Bamboesberg Member was deposited by ephemeral sandy streams with locally established peat swamps (Christie, 1981; MacDonald, 1993 Hancox, 1998). According to Christie (1981), this basal member is dominated by arenaceous fine- and medium-grained sandstones interbedded by siltstone, mudstone clasts and two main coal seams (Guba and Indwe) formed in swamps (Figure 7).

2.3.2 Indwe Member

The Indwe Member comprises very coarse-grained sheet-like sandstone coarsening upwards (Christie, 1981; Hancox, 1998). The sandstones are distinguished by the overgrowth of quartz that brings a unique glittering appearance to the sandstone (Christie, 1981). The upper part of the member comprises alternating layers of fine- and medium-grained sandstone. According to Christie (1981), the Indwe Member was deposited after the source area rose rapidly, creating a fast-moving water current capable of carrying coarser sediments. The member does not contain any coal seams (Turner, 1975; MacDonald, 1993).

2.3.3 Mayaputi Member

The Mayaputi Member sediments were deposited when tectonic activity was reduced at the source, resulting in distal floodplain deposits that transgressed southward over the more proximal braided-stream deposits. This member is mainly composed of mudstone (shale and siltstone) and fine-grained sandstone at the base and overlies the Indwe Member. In addition, this member hosts the Molteno coal seam (also known as the Cala Pass-, the Cala-, Piet-, or Upper seam) (Turner, 1975; Christie, 1981; MacDonald, 1993).

2.3.4 Qiba Member

Christie (1981) suggested that the Qiba Member sediments were deposited by high-energy transient currents. It comprises a series of fine- to medium-grained sandstone beds with mudrock parting and it hosts a coal seam with a shaly inconsistency named the Gubenxa seam (also known as the Ulin seam).

2.3.5 Tsomo Member

The Tsomo Member represents the alternation of different periods, one period of strong tectonic activity resulting to coarse sandstone, and the second period of limited tectonic activity resulting in a mudstone deposition (Christie, 1981; MacDonald 1993).

2.3.6 Loskop Member

The uppermost member of the Molteno Formation, the Loskop Member, comprises coarse-grained, pebble sandstone, argillaceous units and several thin shaly coal seams, including the Umnachean and Offa coal seams, which are not of any economic significance (Turner, 1975; Christie, 1981;). This member is overlain by reddish-coloured mudstones of the Elliot Formation.
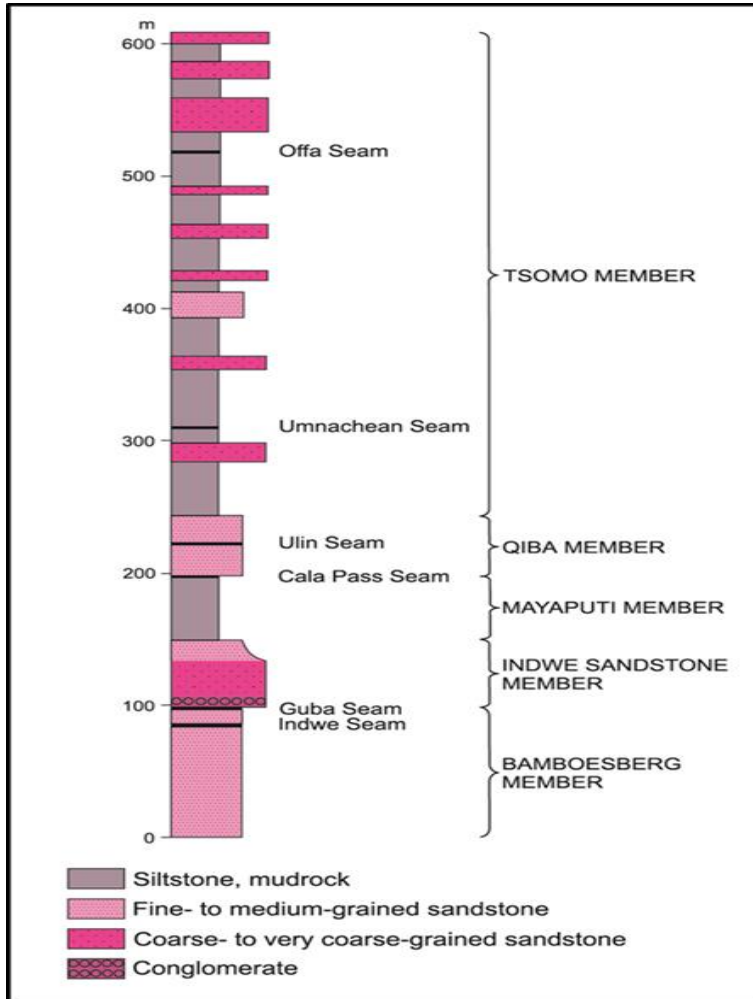
Figure 7. Typical section of the Molteno-Indwe coalfield in the southern outcrop area (Christie, 1981).

2.4 Coal Seams of the Molteno–Indwe coalfield

There are six coal seams within the Molteno Formation, from the base up these being the: the Indwe, Guba, Molteno, Gubenxa, Umnachean, and Offa Seams (Figure 8) (Christie, 1981).

2.4.1 Indwe Seam

The Indwe Seam occurs within the Bamboesberg Member at approximately 24-30 m from the top (Christie, 1986). The seam contains many mudrock partings and the coal is mainly dull or dull-lustrous (MacDonald, 1993) and it attains maximum thickness of 4.3 m just north of the Indwe district.

2.4.2 Guba Seam

The Guba Seam also occurs within the Bamboesberg Member and is situated between 10 and 30 m above the Indwe Seam (Christie, 1981). The seam has a higher coal: shale ratio than the Indwe Seam. It attains its maximum thickness of 2.7 m in the Guba area, approximately 10–15 km south-west of Indwe town. The coal is either dull or dull-lustrous with bright bands (Heinemann and Buhmann, 1987; MacDonald, 1993).

2.4.3 Molteno Seam

The Molteno Seam, also known as the Cala Pass Seam, occurs within the Mayiputi Member at approximately 30 m to 50 m above the Guba Seam. Although this seam is named after the town of Molteno, there is no record of the seam being developed within the Molteno district; this suggests that there might be a misnomer. Its thickness rarely exceeds 0.6m and contains approximately 50% shale partings (MacDonald, 1993). The seam is extensively developed between Ugie, Cala, and Engcobo, but the thickness is variable.

2.4.4 Gubenxa Seam

The Gubenxa Seam developed within the Qiba Member, approximately 30–40 m above the Molteno Seam (MacDonald, 1993). The seam is very shaly and contains no more than 40% clean coal at most localities.

2.4.5 Umnachean and Offa Coal Seam

These are minor coal seams within the Loskop Member. Usually occurs as thin bands of coal (less than 0.1 m thick) and is sporadically bright.
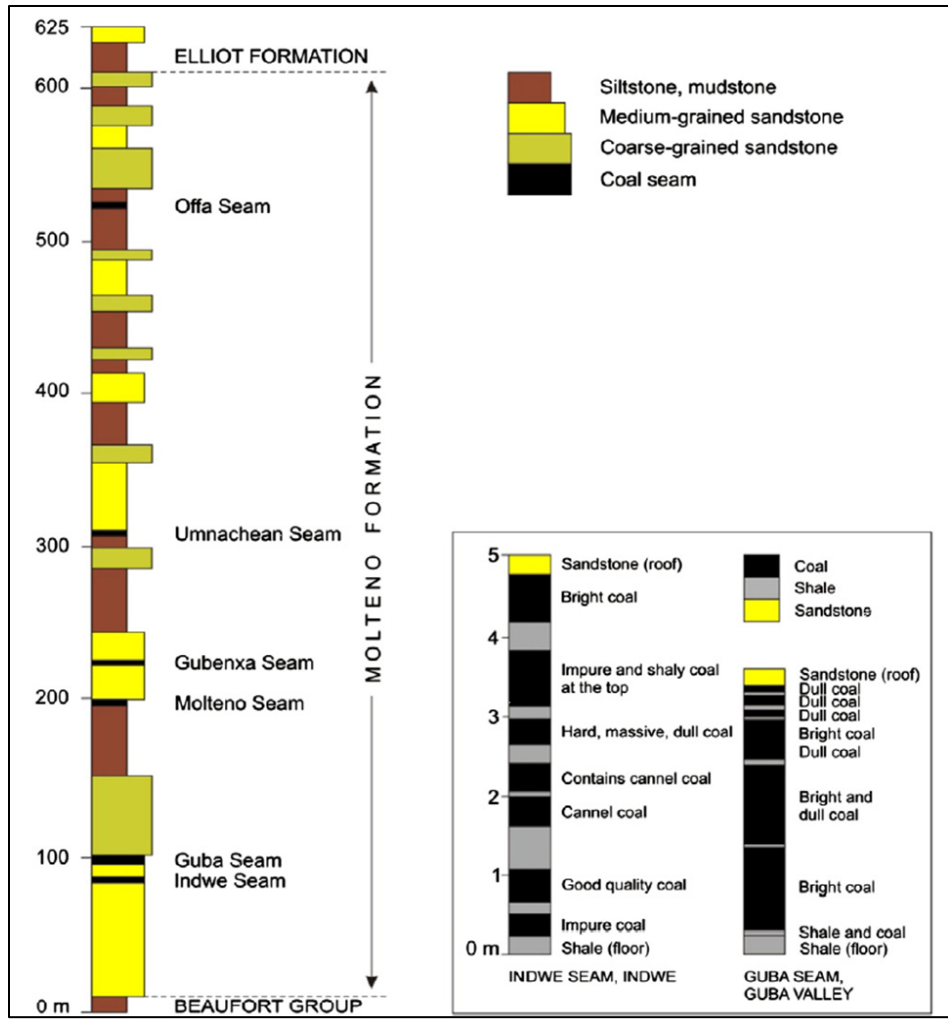
Figure 8. Composite stratigraphic column for the Molteno Formation (Christie, 1981).

2.5   Braided River Architecture

The Molteno Formation was deposited by network river systems, which consist of channel segments that divide and reconnect around bars and islands (Turner, 1975; Eriksson, 1984; Christie, 1981). These systems are important deposition agents, resulting in sedimentary sequences like aquifers, hydrocarbon reservoirs, and heavy mineral accumulation (Bristowet al., 1993). Miall (1977, 1978). Various researchers (Ore 1964; Smith 1970; McKee et al., 1967; Coleman 1969; Williams and Rust 1969) have significantly contributed to the study of braided river deposits.

Miall (1977, 1978) presented six vertical sedimentation models for braided stream deposits. These models are illustrated in Figure 9 and include small-scale cyclic sequences indicated by arrows.

Interpretation of the stratigraphic succession of ancient braided-river deposits indicates similarities between the Bamboesberg Member and Bijou Creek-type deposits (Christie (1981). These similarities include scoured basal surfaces, intraformational conglomerate beds, planar stratification, and a prevalence of sandstone composition. The presence of lenticular argillaceous intercalation of beds is also a common feature. Not much argillaceous sediment was found in both successions, suggesting limited preservation of argillaceous strata (Christie (1981).

Figure 9. Vertical profile models for braided stream deposits. Facies codes to left of each column and arrows show small-scale cyclic sequences (Miall, 1977).

3 Materials and Methods

3.1 Methodology

A total of thirteen vertical boreholes drilled in the Molteno-Indwe coalfield between 1984 and 1986 were selected and retrieved from the Council for Geoscience National Core Library at Donkerhoek. These cores were selected based on their geographical distribution within the coalfield and because they are dominated by the lithology of the Bamboesberg Member. The selected cores were logged in detail and scanned by hyperspectral imaging scanner. Fourteen sandstone samples were collected from the logged cores and analysed for physico-chemical including petrography, XRF (X-ray fluorescence) and scanning electron microscopy (SEM), energy dispersive X-ray analysis (EDX) (SEM-EDX). The geological fieldwork was conducted to collect the coal samples within the Bamboesberg Member and to profile the Bamboesberg Member lithology.

Figure 10. Core trays laid out at the national core library for logging and sampling. Generally, mudstone is broken and disaggregated while the sandstones are still intact.

3.1.1 Sampling and field work

Extensive geological fieldwork was conducted, with a particular emphasis on exploring the sedimentation cycles of the Bamboesberg Member within the Molteno Formation. The fieldwork involved coal sampling, meticulous recording of photographs, elevation, and coordinates to ensure accurate analysis and representation of the data. Most of the outcrops visited are exposed along the road cuts (Figure 11). GPS and topographic maps were used to navigate to the sampling points. In addition, the coordinates of each sample point were marked by GPS and later transferred and combined into an excel spreadsheet.
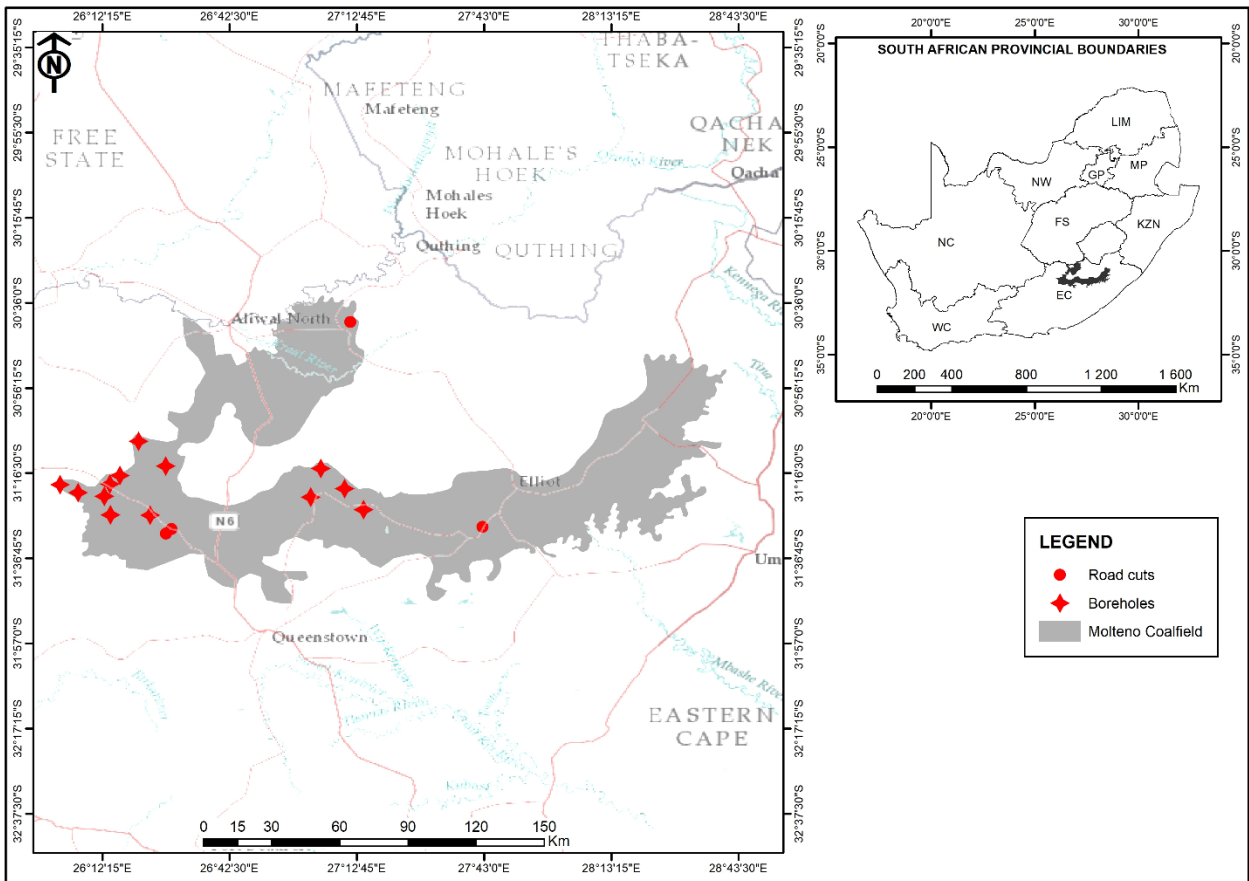
Figure 11. Map showing location of logged boreholes and exposed road cuttings.

3.1.2 Hyperspectral imaging scanner

A hyperspectral imaging scanner was employed to determine the mineral composition of the selected cores (Figure 13).

Figure 12. An image of the core trays scanned at the national core library using a hyperspectral-imaging scanner.

3.1.3 Petrography

A thin section of each sandstone sample was prepared in the Council for Geoscience's laboratory. Analyses were performed using a petrographic microscope with an inbuilt camera and software that captured photomicrographs at X40 magnification.

3.1.4 XRF (X-ray fluorescence)

Sandstone samples were submitted to the Council for Geoscience's laboratory to determine the concentration of major elements using the XRF machine. The sandstone samples were crushed and milled. For major element analysis, the milled samples ($<75\ \mu$ fraction) were first dried for at least 3 hours at 100 °C and then roasted at 1000 °C for at least 3 hours to oxidise Fe_2+ and S, which is detrimental to the Pt ware used to prepare glass disks. The loss on ignition (L.O.I.) and moisture (H_2O) were determined gravimetrically during the drying and roasting steps. The glass disks were prepared by fusing a 1 g roasted sample with a 10 g flux consisting of 49.50% $Li2B_4O_7$, 49.50 $LiBO_2$, and 1.00% LiBr at 950 °C. The glass disks were then analysed by a PANalytical Axios X-ray fluorescence spectrometer (XRF) equipped with a 4 kW Rh tube. Mrs. Corlien Cloete from CGS laboratory conducted the XRF analyses according to Cloete and Truter (2001).

3.1.5 Inductively Coupled Plasma Mass Spectroscopy (ICP-MS)

The South African Bureau of Standards (SABS) in Secunda, Mpumalanga, assessed the concentration of rare earth elements in coal samples using Inductively Coupled Plasma Mass Spectroscopy (ICP-MS).

Thirty-eight coal solid samples were prepared by mixing pulverised coal samples (<200 mesh) with calcined $LiBO_2$ (lithium borate) at a ratio that varied from 1:10–1:4 until optimised recoveries were determined. The crucible containing the sample was then heated at a low temperature for 1–2 minutes. The sample mixture was heated to initiate and speed up the oxidation reaction that would follow soon after. Distilled water was slowly added to the sample mixture to initiate oxidation between the sample and the base.

The fusion was carried out at a high temperature of around 1000 °C using an automatic fusion fluxer. At this high temperature, the sample was melted and dissolved by the lithium borate flux to form a perfectly homogeneous mass. The glass was digested in 5% HNO_3 on low heat while the sample was continuously stirred. The platinum crucibles were rinsed in triplicate with 5% HNO_3 to ensure that the sample glass was completely digested and the sample was diluted to a final volume of 100 ml. The samples were further diluted between 10 and 100 times in 2% HNO_3 before analysis to determine the optimal balance between internal standard recovery and the limit of detection. For each set of fusions prepared for this study, blank samples containing only lithium borate were prepared and processed in the same way for quality assurance and quality control.

3.1.6 Scanning electronic Microscope (SEM)

Twelve representative sandstone samples were analysed using scanning electron microscopy (SEM) and energy dispersive X-ray analysis (EDX) to understand the spatially resolved mineralogy. A total of eight coal samples, which showed a high concentration of REE, were analysed by the SEM-EDX to determine the host-bearing REE minerals in the coal samples collected within the Bamboesberg Member. Both sandstone and coal sample analyses were performed at the Council for Geoscience Laboratory in Silverton, Pretoria.

A polished, thin section was prepared for each sample and carbon-coated. A Zeiss Sigma 200 VP scanning electron microscope with a Bruker energy-dispersive x-ray spectrometry (EDX) detector was used for the analysis. Backscattered electron (BSE) images were captured to show the mineral occurrences and mineral identification was carried out using standard-less EDS.

3.1.7 3D Modelling

Thirteen selected cores together with the stratigraphy lithology collected from the road cuttings were used to create the 3D modelling of the study area, using leapfrog software 4.1. The model provides information about the geographic distribution of lithostratigraphic units in the Bamboesberg Member.

4 Sedimentology

4.1 Introduction

This chapter presents comprehensive lithologic descriptions of the sandstones of the Bamboesberg Member of the Molteno Formation using thirteen vertical boreholes that were drilled within the study area, with depths ranging from 46 to 132 m. lithological, the boreholes are dominated by sandstone beds interbedded by mudstones and coal interspersed in some places. Although the sandstones remain intact, the mudstones and coals are highly weathered and oxidised (Figure 10)**.**

4.2 Lithology and sedimentary structures

The Bamboesberg Member is distinguished by fining upward cycles of sparkling sandstone interbedded with argillaceous units capped by coal in places, as observed in both cores and in the field. These observations are consistent with those of Christie (1981) and Hancox (1998). According to Hancox (1988), the glittery appearance of sandstone in sunlight is explained by the growth of quartz crystals in optical continuity with detrital sand grains. Argillaceous units are dark grey to blackish or yellowish grey, depending on the quantity of silt and carbonaceous material in them. Shales are generally more fissile and contain plant remnants locally (Christie, 1981). Dolerite intrusions observed on cores SF1/85, CG1/85, MF1/85, PP5/86 and UK1/85 (Figure 14). Dolerite intrusions form baked material on mud rocks/siltstone contact, whereas they form slight metamorphism at the sandstone contact.

All the logged cores show a phenomenon of fining-upward in grain size per cycle and coarsening-upward in the overall Bamboesberg Member succession is clearly visible (Figure 14, 15 and 16). This distinctive phenomenon has also been mentioned by other researchers within the studied succession. (Rust, 1962; Turner, 1971; Christie, 1981; Hancox, 1998;). Coal seams and baked material due to dolerite intrusion were also observed in the cores (Figure 14).
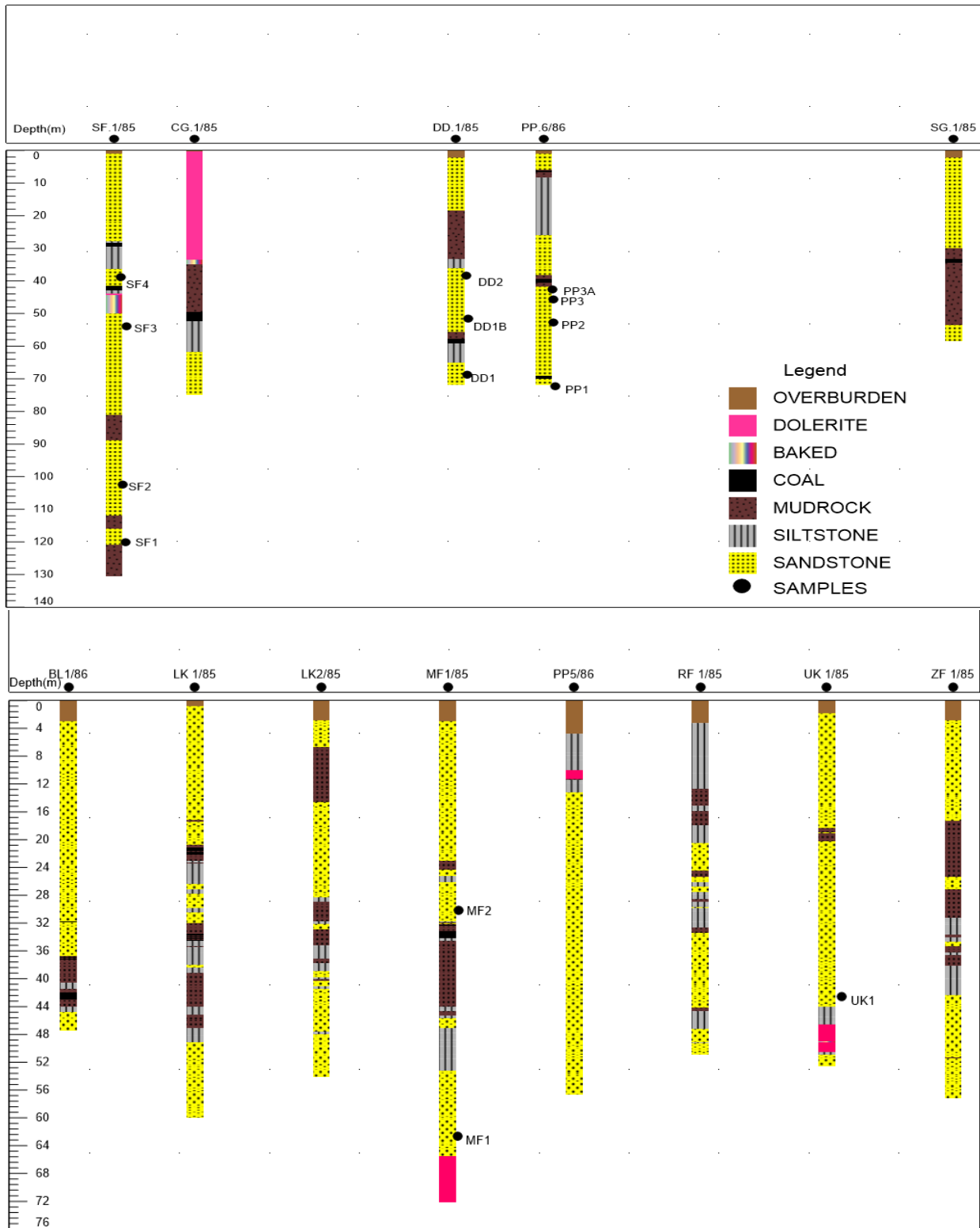
Figure 13. Lithology of the logged thirteen drill cores with sampled points.

4.2.1 SF1/85

Core SF1/85 comprises four sandstone cycles, dominated by faint horizontal and cross stratification with mud intraclasts in places. The core depth is 132m.

The second sandstone cycle at the base, emerging from the argillaceous unit of the first sandstone cycle, comprises medium grains grading upwards to very fine grains, poorly to moderately sorted, yellow grey (5Y 8/1) and light grey (N7) in places. An 11-meter-thick sandstone strata rests on mudrock with an erosion contact, whereas the top contact is gradational to mudstone.

The third sandstone cycle comprises medium to coarse grained strata at the base, grading to medium then fine upwards, moderately sorted. The sandstone unit is approximately 22 m thick and medium grey (N6). The lower contact with the mudstone is sharp, whereas the upper contact with the siltstone is gradational.

The fourth sandstone cycle comprises medium grained strata at the base grading to fine / very fine at the top, well sorted, medium grey (N6) to light grey (N7). The sandstone cycle forms large-scale structures about 38.6 m thick with siltstone beds in places up to 90cm. The lower boundary is erosional and the upper boundary is in sharp contact with dolerite intrusion. The upper contact with the dolerite appears faintly metamorphosed. The intersection of dolerite intrusion is encountered at 47.7m. The dolerite intrusion appears to have baked the mudrock and Indwe coal seam at 44.6m - 42m (Figure 16).

The fifth sandstone cycle comprises medium grain strata at base grading to fine at the top, moderately sorted, yellow grey (5Y 8/1) to light grey (N6-N7). The sandstone thickness is about 3m. The lower and top boundaries are gradational. This cycle is fining upwards to siltstone, then to the Guba seam.

Figure 14. Vertical profile and sedimentary structures of core SF1/85.

4.2.2 LK1/85

This core, drilled at a depth of 60 m, comprises two sandstone cycles of the Bamboesberg Member capped by Indwe Member units.

The fourth sandstone cycle consists of medium grained strata at the base grading to fine grains, moderately sorted, light grey (N7). The sandstone unit is about 9 m thick; the upper contact is gradational to siltstone. The Indwe coal seam horizon occurs within this cycle at a depth of 33.54 to 34.6 m.

The fifth sandstone cycle consists of medium- to fine-grained strata at the base to fine-grained at the top, with mudstone and siltstone intra-clast inclusions in places, moderately sorted, light grey (N7). The sandstone thickness is 11.1 m and overlies mudstone with an erosional contact, while the upper contact is gradational to siltstone. The Guba coal seam horizon occurs at a depth of 21.15 m to 22.15 m.

Indwe Member from 1.8m to 22.3 m overlies the Bamboesberg Member with a sharp contact and consists of medium to coarse grains, yellow brown (10 YR 5/4) with orange pink stains (5 YR 8/4). The lower contact with the Bamboesberg Member is sharp.
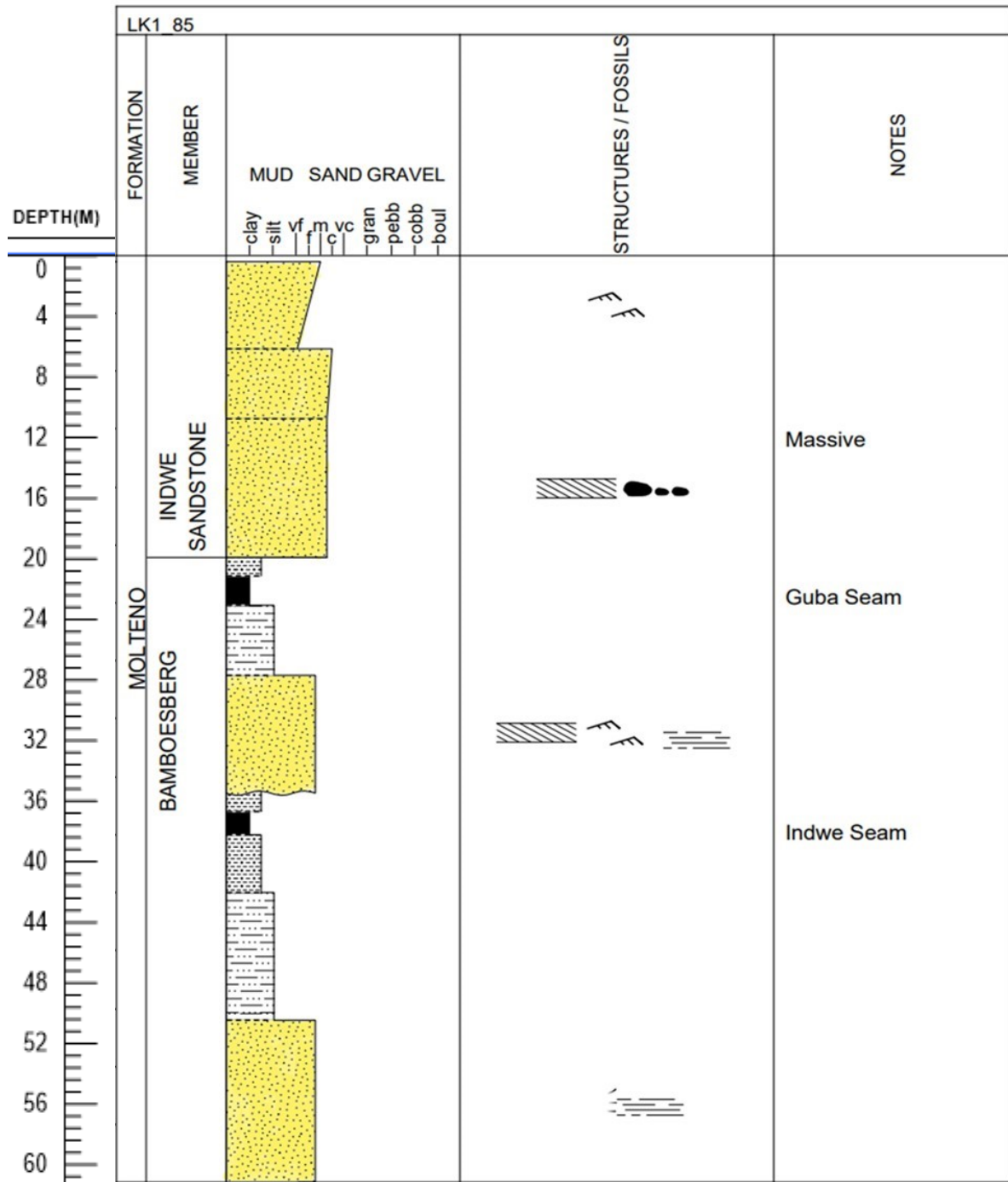
Figure 15. Vertical profile and sedimentary structures of core LK1/85.

4.2.3 PP6/86

The PP6/86 core drilled at a depth of 72.03 m comprises sandstone cycle four of the Bamboesberg Member, capped by the Indwe Member.

The fourth sandstone cycle at the base of the core consists of medium-grained strata at the base and fine grains at the top, light grey (N7) to medium grey (N6). This sandstone unit is about 2 m, grading upwards to siltstone. The Indwe coal seam horizon occurs at 69.05 to 70.15 m.

The fifth sandstone cycle consists of medium grains at the base to fine-grained strata at the top, light grey (N7), moderately to poorly sorted in places. The sandstone unit is about 23.01 m thick and overlies mudrock with a sharp contact, whereas the upper contact is gradational to siltstone then to mudstone. The Guba seam horizon occurs at 40.6 to 40.9 m.

The Indwe Member overlies the fifth sedimentation cycle of the Bamboesberg Member with sharp contact. This member occurs at a depth of 26.88 to 39.38 m and consists of sandstone units of medium-, coarse-, and very-coarse-grained, light brown (5YR 6/6), moderate yellow brown (10YR 5/4), and moderate reddish orange (10R 6/6).

Mayiputi Member is characterised by fine to very fine-grained mudrock strata from the surface to 26.88 m. Cala Pass/Molteno seam horizon formed at 6.10 to 6.70 m.
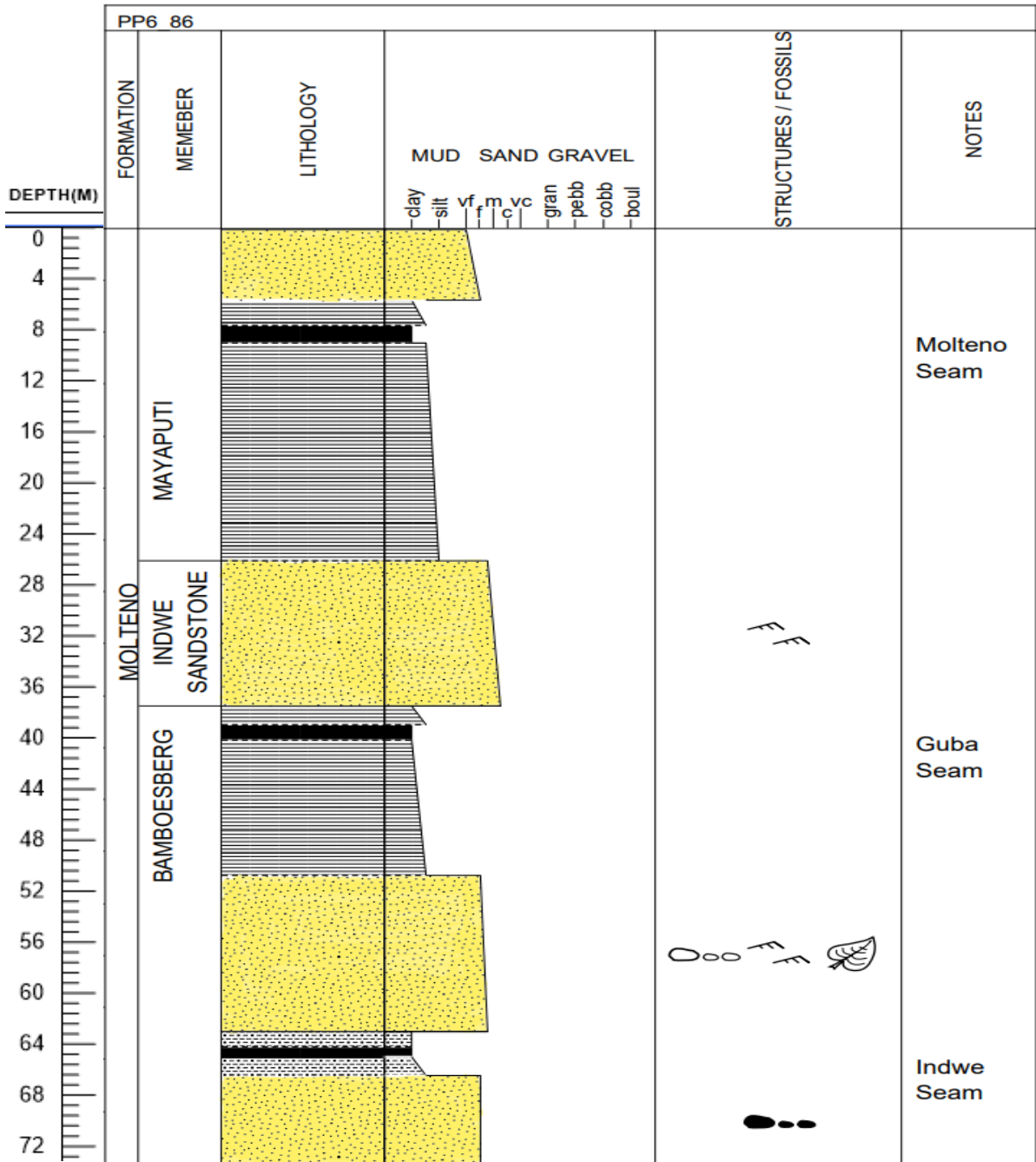
Figure 16. Vertical profile and sedimentary structures of core PP6/86.

4.3   Facies description

Geological characterisation involves a comprehensive interpretation of depositional environments and sedimentary facies. Facies analysis is crucial for reconstructing the stratigraphic evolution in sedimentary deposition environments (Mail, 1996). These facies are generated by various sedimentary processes, including fluid flow, sediment gravity flow, soft-sediment deformation, and biogenic activity (Boggs, 2001). Both lithological stratigraphy and facies play a vital role in geological characterisation studies as they provide tools for analysing ancient depositional settings and representing the environmental conditions that existed during or shortly after deposition. Sedimentary features (facies) can be used to evaluate sediment transport processes, paleocurrent flow directions, relative water depths, and relative current velocities in ancient sedimentary settings (Boggs, 2001; Miall, 1977).

The facies analysis presented in this study focuses on the sandstone units of the logged cores representing the Bamboesberg Member. It is worth noting that some of the facies may not be evident in core despite their presence in the field. Table 2 provides a summary of the facies codes, sedimentary structures, depositional processes, and depositional interpretations. The terminology used for facies is based on Miall (1977; 1988). Photographs of each observed facies are presented below. The sandstone lithofacies exhibits a variety of stratifications, reflecting the complex depositional environment in which it formed. Among the different types of stratification observed, the primary ones include massive sandstone (Sm), horizontal stratified (Sh), planar cross-stratified sandstone (Sp), and ripple stratification sandstone (Sr). These various stratifications provide valuable insights into the sedimentary processes that occurred during the formation of the sandstone lithofacies. The presence of these distinct stratifications suggests different flow conditions and depositional environments, each leaving its unique imprint on the sandstone.

Table 2. A summary of facies code, sedimentary structures, depositional processes and depositional interpretations.

Facies code	Sedimentary structures	Depositional process	Interpretation
Sp	Planar cross-stratification sandstone	Mid to high energy, unidirectional traction sedimentation	Channel-fill sands
Sh	Horizontal stratification sandstone	Planar bed deposition near or at the upper flow regime	Planar bed deposition near or at the upper flow regime
Sr	Ripple cross-stratification sandstone	Lower flow regime, during waning flood and slack water conditions	ripples (lower flow pattern)
Sm	Faintly or Massive - stratification sandstone	Rapid suspension fallout	Suspension deposition during flood events
Fl	Laminated sandstone, siltstone and mudrock		Suspension deposition during flood events.
C	Coal	Peat accumulation and coalification	Raised, floating, or low-lying mire
DO	Dolerite intrusions as sills and dykes	Basic igneous intrusions	Jurassic-age igneous

4.3.1 Planar cross-stratification sandstone (Sp) facies

Description

Facies Sp is one of the distinctive features of these sandstones, occurring as fine- to medium-grained sediment (Figure 17A). This facie is commonly found within the study succession and is often associated with ripple stratification, adding to its unique characteristics. The sandstones displaying planar cross-stratification can be observed in light to medium grey shades (N7-N6). It is noteworthy that this facies typically occurs in grouped sets with inclination that varies from 18 to 30 degrees. The lower boundary of the stacked planar cross bedding demonstrates either a gradual transition to horizontal stratification sandstone (Sh) or ripple-cross laminated sandstone (Sr), indicating the intricate nature of sedimentary deposition. On the other hand, the upper contact of this facies generally exhibits a grading towards faintly Sh, indicating potential changes in sedimentary dynamics.

Interpretation

Planar cross-stratification is primarily formed through the downstream migration of two-dimensional bed forms. These bed forms, characterised by their flat and parallel layers, are observed to occur during low flow regime conditions, as highlighted by Boggs, (2001) and Melehan et al. (2021).

4.3.2 Horizontal stratification on sandstone (Sh facies)

Description

The facies (Sh) horizontal stratification is a one of the prominent features within the studied succession and is observed in all logged cores. Observed in fine to medium grained, light (N7) and medium grey (N6) sandstones (Figure 17B). This particular facies (Sh) is characterised by the presence of faint foreset laminae, comprising dark grey to black carbonaceous material. It is noteworthy that the top and bottom contacts of this facies exhibit a general gradational contact with either Sm and or Sp. Interestingly, in certain locations, this facies observed to coexist with planar cross lamination, adding complexity to its overall composition. The horizontal stratification, on the other hand, appears to form a large-scale pattern with varying thicknesses, ranging from 0.1 to 1 m. The study of these distinct features provides valuable insights into the stratigraphic evolution and sedimentary dynamics of the studied succession.

Interpretation

The Sh stratification is a result of the deposition of sediment particles on the upper flow regime plane beds. These sediments are typically composed of fine-grained particles such as silt and clay. The deposition of these particles leads to the formation of distinct layers or stratifications within the sedimentary deposits (Boggs, 2001; Christie, 1988).

4.3.3 Ripple wave stratification Sr on sandstone (Sr facies)

Description

Ripple (Sr) wave stratification was observed in the logged cores. It consists of very fine- to fine-grained, moderately to poorly sorted sandstone arranged into trough-cross-bedded sets and cosets (Figure 17C), 2–40 cm. It is commonly associated with Sp.

Interpretation

Sr Stratification formed when water movement over a sandbed, as unidirectional currents, as oscillatory waves or as a combination of both, may give rise to ripples.

Figure 17. (A) Cross-stratification Sp stratification sandstone, core: PP5/86. (B) Horizontal Sh stratification sandstone, core: PP5/86). (C) Ripple wave Sr stratification sandstone, core: (BL1/85). Tape Measure scale is in centimeters.

4.3.4 Massive or faint graded sandstone (Sm facies)

Description

These sandstone units appear to be structure-less for the most part, although it is conceivable that they are stratified. The facies Sm appears to consist of what initially appeared to be homogeneous sandstones. However, upon closer inspection, it is evident that this facies includes small, irregular lenses, these lenses appear to have smaller grain size compared to the overall composition of the rock. This characteristic has been observed in all the studied cores. The facies Sm is predominantly composed of seemingly massive fine- to medium-grained sandstones with a yellow-grey colour (5Y/8/1) (Figure 18A). These sandstones are moderately sorted and can vary in colour from light (N7) to medium grey (N6), depending on the relative amounts of feldspar or rock fragments present. The bottom contacts of this facies typically exhibit extrabasinal clasts, which are more common than local mud intraclasts. The beds within these facies are generally unstratified and can span a considerable scale, ranging from 5 cm to as much as 1.2 m.

Interpretation

The lack of structures within the sandstone occurs in the absence of traction transport and results from very rapid deposition from suspension or deposition from very highly concentrated sediment dispersions during sediment-gravity flows (Boggs, 2001).

4.3.5 Sedimentary structure: Graded bedding

Description

The bed grading phenomenon observed within the studied succession, typically indicating the transition from fine-grained to coarse-grained deposits, which is considered a normal occurrence. However, reverse grading, where the transition is from medium-grained to fine-grained, is also present but is a relatively rare occurrence (Figure 18B). However, reverse grading, where the transition is from medium-grained to fine-grained, is also present but is a relatively rare occurrence.

Interpretation

Normal grading can be formed by several processes such as sedimentation from suspension clouds generated by storm activity on the shelf or deposition in the last phases of a heavy flood, but the origin of most such graded beds in the geologic record has been linked to turbidity currents (Boggs, 2001). Reverse grading is not a common phenomenon within the studied succession. Reverse

grading normally results from deposition by a fast-moving debris flow (Boggs, 2001; Melehan et al., 2021).

Figure 18. (A) Massive or faintly stratification sandstone, core: RF1/85. (B) Normal grading sandstone, core: MF1/85). Tape Measure scale is in centimetres.

4.3.6 *Coal facies (C)*

Description

Facies C occurs in sedimentary cycles within the argillaceous material in the studied succession. The coal facies is typically black (N1). Facies C was observed in the core MFI/85 (Figure 19A). As depicted in Figure 19A, the coal sample is covered in plastic to reduce the oxidation rate. However, even with these mitigation measures, the oxidation of this coal over the last few decades has rendered the coal unsuitable for laboratory analysis. Certain features in the coal, such as

slickensides, colour and thickness, can still be discerned. Observations can be made of black swamp peat deposits and areas of plant colonization. The alternating bands of bright and dull coal indicate fluctuations in the water table level.

Interpretation

The deposition and formation of coal facies occur through the accumulation of peat from organic debris in water-logged conditions (Boggs, 2001; Christie, 1988).

This peat, under increasing temperature and pressure after burial, undergoes a transformation into different forms of coal: firstly lignite, then bituminous coal, and finally anthracite (Boggs, 2001). Within the succession studied, facies C has been identified as bituminous coal (Heinemann and Buhmann, 1987; MacDonald, 1993). Whereas Setladi (2023) classified the Guba seam as high rank C anthracite.

Coal stringers

Vestigial coal stringers are moderately common in sandstones within the studied (Figure 19B).

Figure 19. (A) The Guba Seam observed on core: MFI/85). (B) Vestigial coal stringers in the medium-grained sandstone (Core: BL1/85). Tape Measure scale is in centimeters.

4.3.7 *Other features observed: Clasts, Intraclast and Pyrite lenses*

Description

The clasts are disc-shaped, angular to sub-angular mudstone and or siltstone fragments. From the selected cores, the fragments can be up to 4 cm in length (Figure 20A).

Disseminated pyrite and pyrite rings are noted in a fine-grained sandstone. Pyrite rings occur but are rare in the studied succession. These pyrite rings cycle around siltstone nodules (Figure 20B).

Interpretation

The clasts / intraclasts form when high-energy currents rip pre-existing muddy material from the base of the stream, transporting it as clasts and re-depositing it (Boggs, 2001). These siltstone clasts are greenish-grey in colour and angular to sub-angular in shape (some clasts show soft deformation) with an average diameter of 1–2 cm.

Figure 20. (A) Siltstone rip up clasts within fine-grained sandstone (RF1/85). (B) Siltstone clasts with pyrite ring within the massive fine to medium-grained sandstone (ZK1/85).

5 Results

5.1 Mineral dominant map

The mineral dominant map acquired using the SisuRock hyperspectral-imaging scanner, the first in southern Africa, installed at the National Borehole Core Depository (NBCD) of the Council for Geoscience. Using both long-wave infrared light (LWIR) and short-wave infrared light (SWIR) to produce a visual "map" of the minerals that respond to reflectance principles on the surface of a core (Figure 21). The SWIR is essential in delineating phyllosilicate and clay minerals; most alteration haloes are detected within this wavelength range. Whereas the LWIR identifies primary or rock forming minerals such as tectosilicates, amongst others. In combination, these ranges provide a good mineral detection system. Thirteen selected cores scanned by hyperspectral imaging, to determine a detailed mineral composition of the cores. Only four representative cores containing dominant mineral compositions are presented in this study.
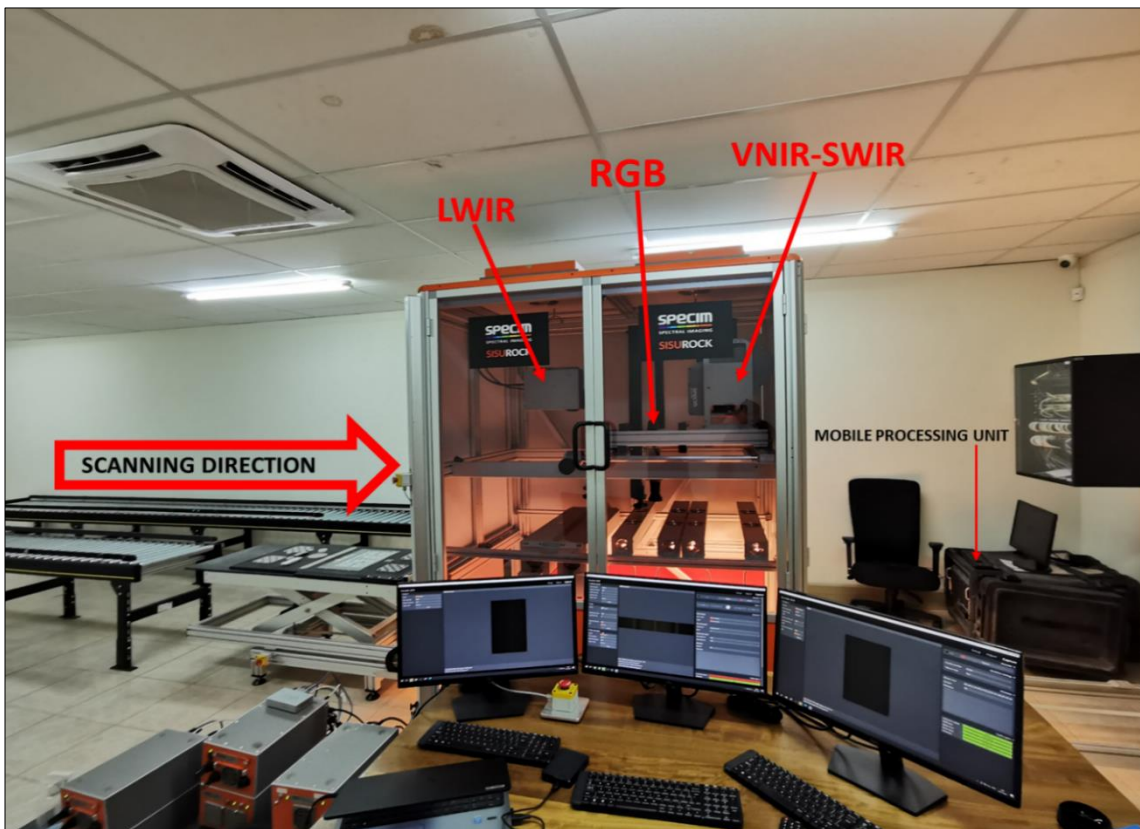
Figure 21. CGS Sisurock system with the LWIR camera (owl), the high-resolution visible light camera (RGB) and the VNIR and SWIR camera (fenix) with co-registered VNIR–SWIR spectrometers.
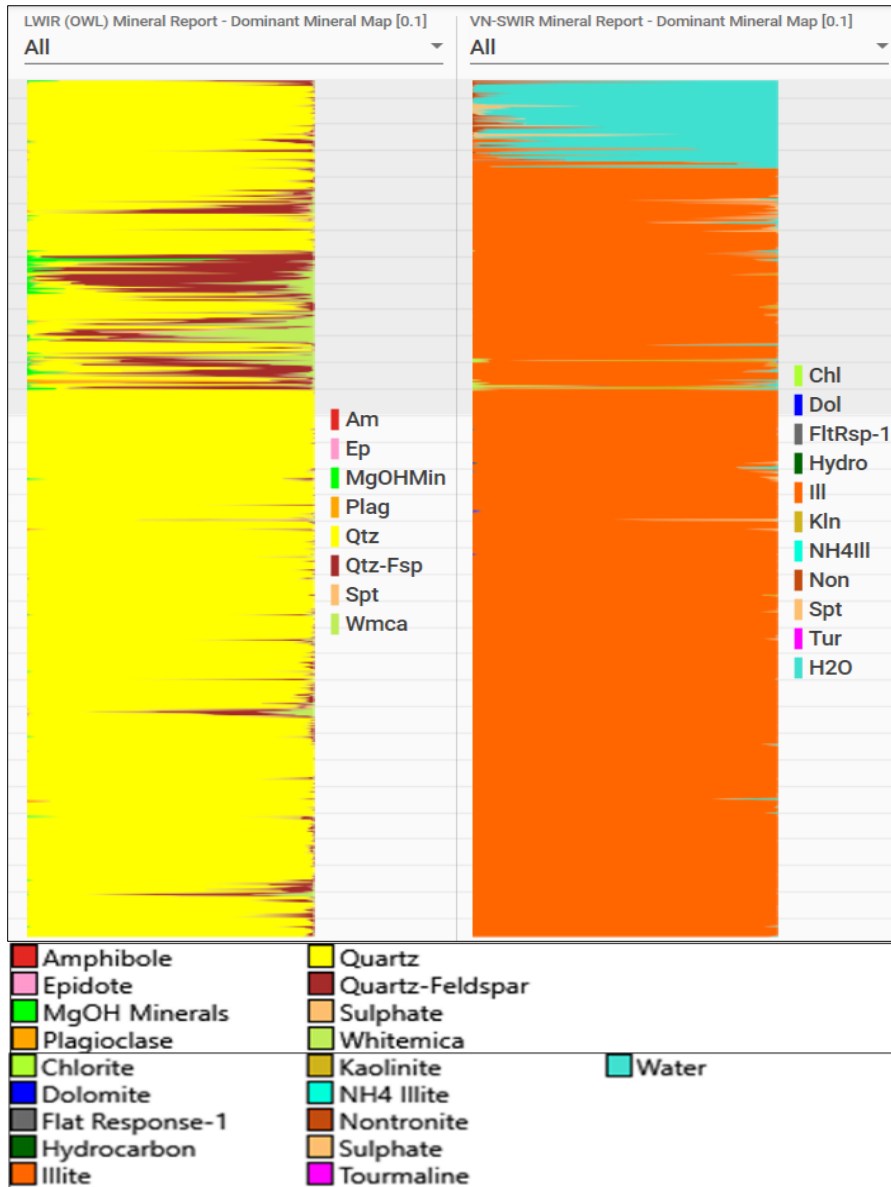
Figure 22. Mineral dominant map of SF1/85.

Mineral groups identified.

LWIR: Mineral dominant map delineates the presence of silicates minerals such as quartz, amphibole, epidote, plagioclase and white mica. Including alteration MgOH minerals. It appears that feldspar occurs more on argillaceous material than in sandstone. **VN-SWIR:** Mineral dominant map revealed the composition of clay minerals such as illite, chlorite, kaolinite, nontronite and tourmaline. Additionally, hydrocarbons and dolomite have been observed (Figure 22).

Figure 23. Mineral dominant map of CG1/85.

Mineral groups identified.

LWIR: Mineral dominant map reveals the composition of silicate minerals such as quartz, white mica, phyllosilicate, including serpentine and sulphate as well as alteration MgOH minerals. **VN-SWIR**: The mineral dominating map shows the composition of clay minerals including illite, kaolinite, nontronite, dickite, and saponite. Additionally, the presence of hydrocarbons and sulphates is observed. Clinopyroxene dominates both LWIR and VN-SWIR, delineating the dolerite intrusion (Figure 23).

Figure 24. Mineral dominant map of BL1/85.

Mineral groups identified.

VN-SWIR: Mineral dominant map reveals the presence of clay minerals such as illite, kaolinite and illite-smectite. **LWIR**: Indicate the presence of silicate minerals which is quartz and muscovite (Figure 24).
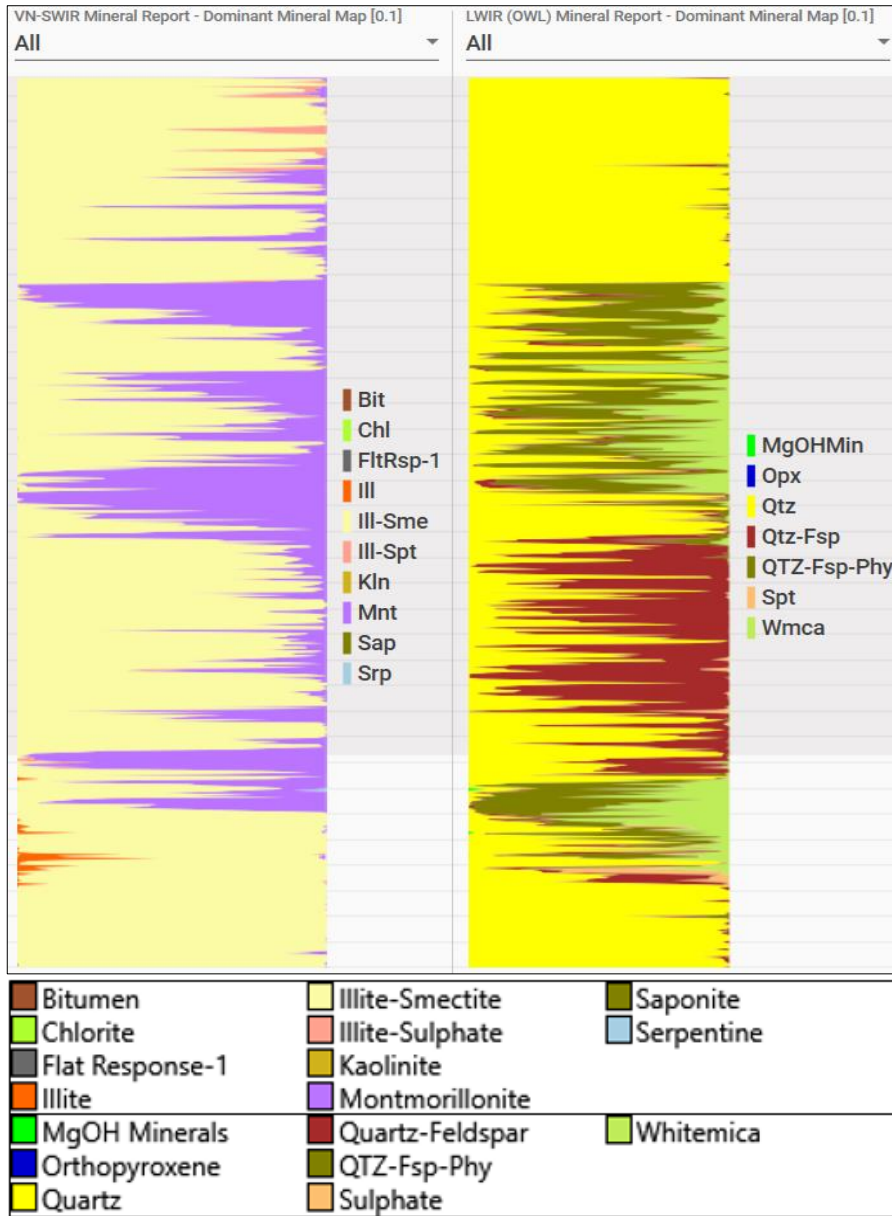
Figure 25. Mineral dominant map of DD1/85.

Mineral groups identified.

VN-SWIR: Mineral dominant map depicts the presence of clay minerals such as illite, kaolinite, illite-smectite, and montmorillonite. **LWIR:** The mineral dominant map shows silicate minerals such as quartz, orthopyroxene, feldspar, and white mica. In addition, sulphates is present (Figure 25).

5.2 Petrography

Petrographic analysis was conducted on eight representative sandstone samples to better understand the characteristics and composition of the Bamboesberg sandstones. The description of the sandstones under a microscope is based on semi-quantitative visual assessments, such as comparison charts for grain size, sphericity, roundness, and sorting (Figure 26). Four representative sandstone samples are presented in this section (SF1, UK1, PP3 and PP1).
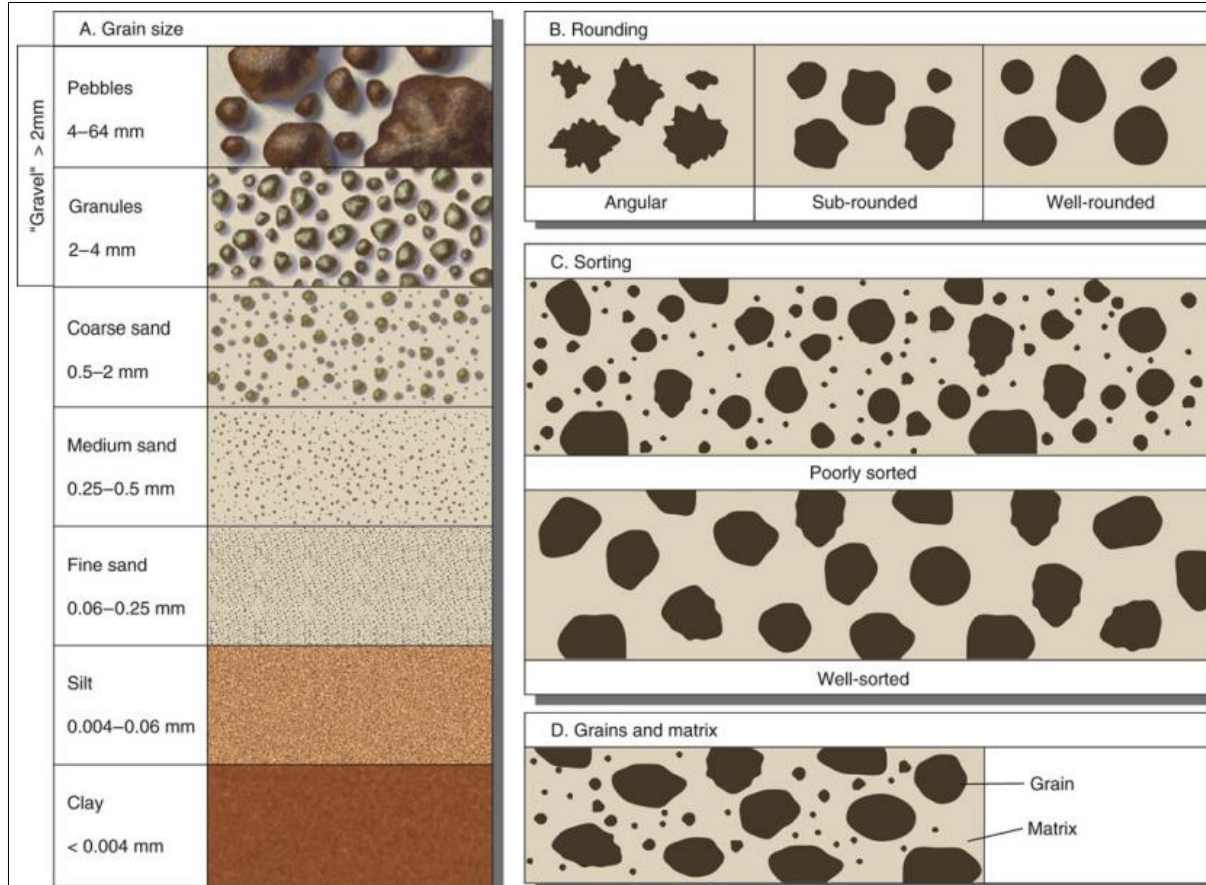
Figure 26. Comparison charts used for the visual estimates of (A) roundness, sphericity and (B) sorting of each sample (after Terry and Chilingar, 1955).

5.2.1 Sample SF1

Sample SF1 was obtained from borehole SF1/85 at a depth ranging from 119 to 120 meters (Figure 12). This sample exhibits poorly sorted and medium grained, the sample is predominantly composed of sub-angular to sub-rounded monocrystalline quartz grains. the presence of mica flakes (specifically muscovite) intermixed with clay minerals serves as the cementing material (Figure 26 SF1). The section primarily comprises around 85% quartz and lithic fragments, with quartz cement also being observed between the grains.

5.2.2 Sample UK1

The sample obtained from borehole UK1/85, taken at a depth of 43.5 to 44m (as shown in Figure 12), reveals interesting characteristics. The UK1 sample showcases a poor sorting pattern, with a medium to fine grain size and an abundance of sub-angular monocrystalline quartz grains. Quartz makes up approximately 82% of the section, while mica flakes can also be observed within the sample. Specifically, muscovite is contorted and appears to be crushed between the quartz grains. Additionally, there are minor plagioclase grains present, exhibiting twinning as depicted in (Figure 26 UK1).

5.2.3 Sample PP3

The sample obtained from borehole PP/86, at a depth ranging from 48.5 to 49 m (Figure 12), exhibits characteristics of poorly sorted, fine-grained sediment. A significant portion of this sediment is composed of very sub-angular monocrystalline quartz grains, accounting for approximately 84% of the section (Figure 27 PP3). Additionally, the presence of chlorite and carbonate as cement material between the quartz grains was observed. Sporadically scattered throughout the matrix are fine-grained quartz grains.

5.2.4 Sample PP1

The sample obtained from borehole PP6/86 at a depth ranging from 71.2 to 71.9 meters (Figure 12) reveals interesting characteristics. It appears to be a mixture of medium to fine-grained particles that are not well sorted. The dominant component in the sample is sub-angular monocrystalline quartz grains, held together by a cement of silica material. In fact, approximately 88% of the composition is comprised of quartz grains, which exhibit micro-cracks upon closer examination (Figure 27PP1). This suggests that the quartz grains may have undergone some stress or deformation over time.

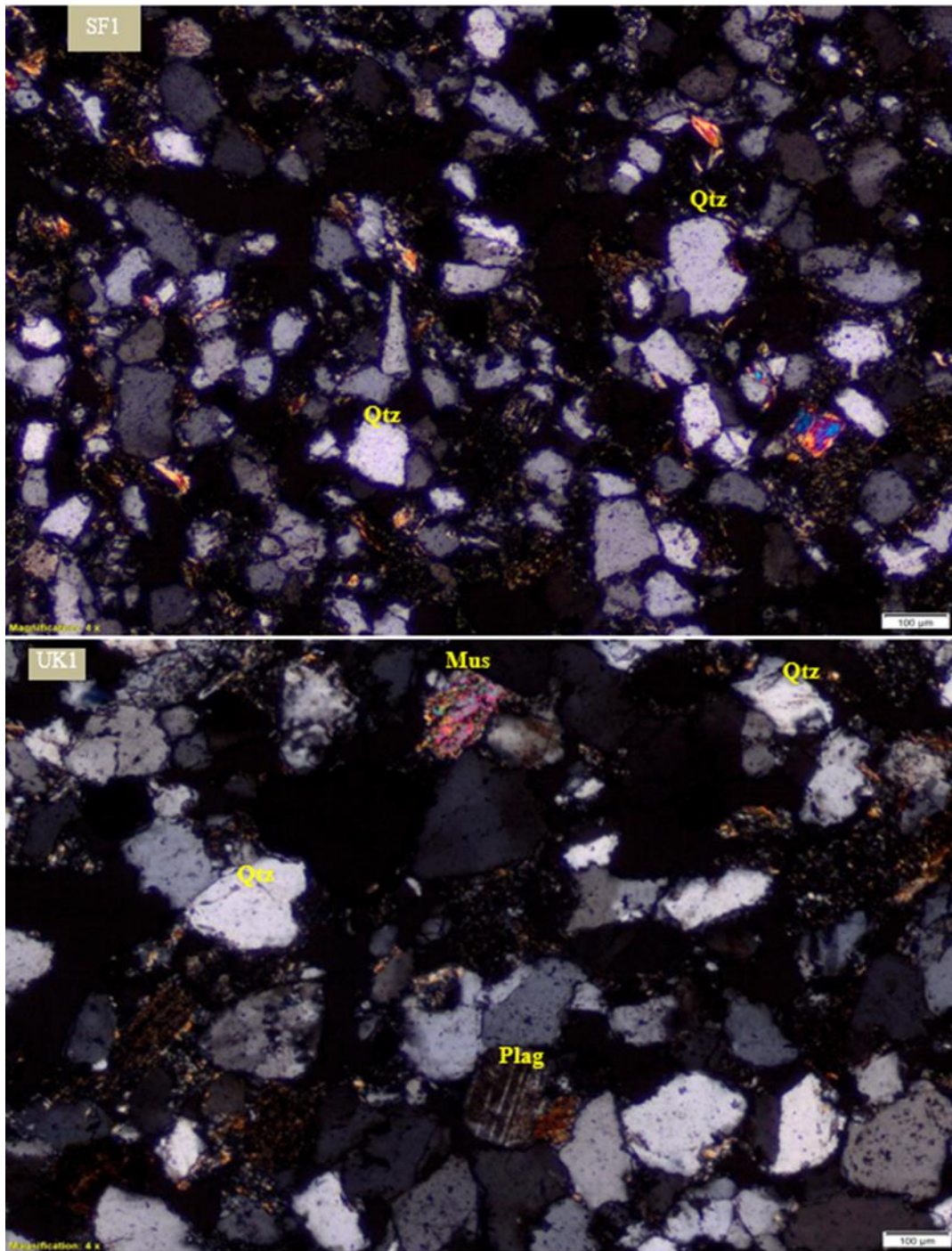**Figure 27. Photomicrograph of sample SF1. Photomicrograph of sample UK1. Both Photomicrographs in cross-polarised light.**
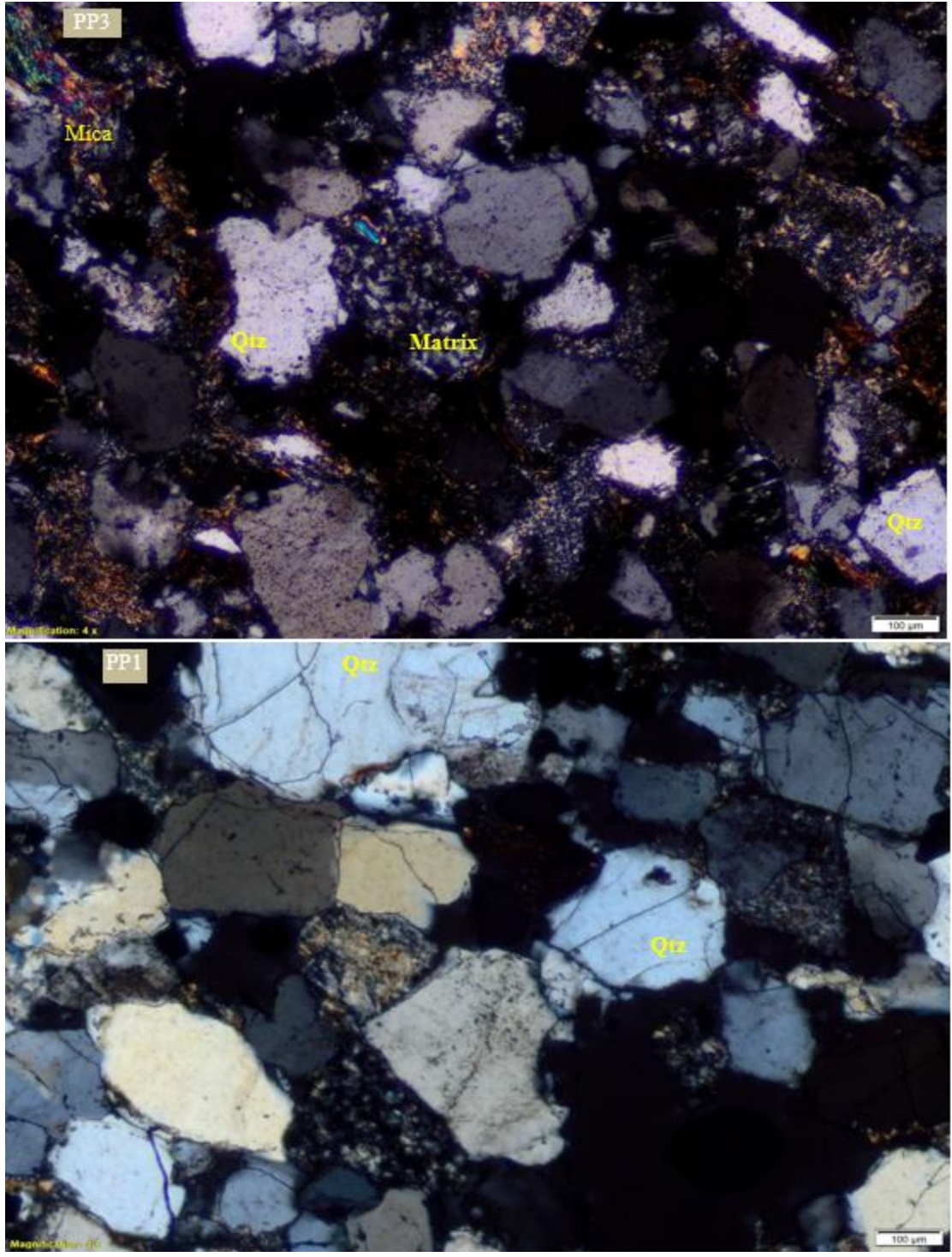
Figure 28. Photomicrograph of sample PP3. Photomicrograph of sample PP1. Both Photomicrographs in cross-polarised light.

Quartz

Quartz, being the most abundant mineral, is present in sandstones. The sandstones are primarily composed of monocrystalline quartz grains (Qm), which are characterised by their sub-angular to sub-round shape and low sphericity. It is intriguing to note that secondary overgrowths of quartz grains are occasionally observed around the original detrital grain boundary. The predominance of monocrystalline quartz grains indicates a recycled sedimentary source or a cratonic source (Al-Harbi et al., 2008; Oghenekome et al., 2018). Therefore, the dominance of monocrystalline quartz grains in sandstones is a significant aspect that supports the idea of a recycled sedimentary source.

Plagioclase

Plagioclase is occasionally observed within sandstones, albeit in lower abundance, indicating a recycled sedimentary source. The rarity of plagioclase can be attributed to various processes, including mechanical abrasion, replacement, dissolution, and sediment reworking, which may have altered or removed it from the detritus. It is worth noting that plagioclase undergoes partial transformation into sericite and chlorite, which are commonly found alteration products of white mica. The plagioclase grains that have been observed exhibit a sub-rounded to round shape with a high degree of sphericity.

Accessory minerals

Mica flakes can be found in various forms, appearing as both fragmented pieces and elongated flakes that are often contorted and crushed between quartz grains (Figure 27PP3). A detailed analysis of petrography has verified the existence of muscovite, chlorite, biotite, and carbonate within these specimens. These minerals were also identified in the dominant mineral map, further supporting their presence in these sandstones.

5.3 Geochemistry

Fourteen sandstone samples collected from the thirteen cores logged were analysed for major elements by X-ray fluorescence (XRF) analysis. The major element composition provides indications of the provenance and weathering conditions of the source that controlled the basin tectonic setting. The major element concentrations are shown in Table 3. The sandstone samples show high concentrations of SiO_2, ranging from 71.85 to 87.56%, followed by Al_2O_3 concentrations ranging from 5.64 to 11.56%.

The Fe_2O_3 concentration ranges from 2.06 to 3.98%. Low concentrations of TiO_2, MnO, and MgO were observed in the sandstone. CaO and Na_2O showed the highest concentrations of 3.41 and 1.17, respectively, on sample DD2, as shown in Table 3. K_2O concentration ranges from 0.9% to 3.01%. P_2O_5 and Cr_2O_3 have very low concentrations.

The presence of Al_2O_3 and K_2O concentrations may be related to the presence of k-feldspars, illite and mica, as detected by the mineral dominant map. The source of Na_2O is mainly related to the presence of plagioclase feldspar (albite). CaO concentration may be related to the presence of calcite, calcium carbonate or anorthite (a calcium-rich end member of plagioclase).

Table 3. Major elements analysis of sandstones as determined by XRF.

Sample ID	SiO_2 %	TiO_2 %	Al_2O_3 %	Fe_2O_3 %	MnO %	MgO %	CaO %	Na_2O %	K_2O %	P_2O_5 %	Cr_2O_3%	LOI %	CIA %	Total %	H_2O %
PP1	87.56	0.29	5.64	2.06	0.04	0.28	0.831	0.75	1.28	0.04	0.005	1.16	66.34	99.93	0.58
PP2	83.32	0.43	8.33	2.32	0.04	0.44	0.651	0.78	1.86	0.08	0.006	1.48	71.68	99.74	0.74
PP3	85.26	0.29	7.35	2.57	0.02	0.29	0.204	0.68	1.81	0.05	0.01	1.24	66.92	99.78	0.71
MF1	84.4	0.37	8.1	2.42	0.03	0.62	0.149	2.59	0.90	0.04	0.007	0.69	69.04	100.32	0.57
PP3A	80.21	0.44	10.26	2.62	0.03	0.59	0.247	0.71	2.49	0.06	0.006	1.97	74.85	99.64	0.89
UK1	84.58	0.46	7.56	2.58	0.04	0.49	0.266	0.66	1.67	0.04	0.018	1.09	74.43	99.45	0.93
SF1	80.33	0.63	10.58	2.95	0.03	0.61	0.223	0.75	1.87	0.07	0.007	1.83	79.00	99.88	1.25
SF2	84.55	0.63	7.11	3.19	0.04	0.61	0.339	0.68	1.25	0.06	0.007	1.1	75.81	99.57	0.8
SF3	83.11	0.48	9.27	2.55	0.02	0.53	0.17	0.07	2.1	0.02	0.013	1.37	79.85	99.7	1.17
MF2	79.09	0.51	10.34	3.98	0.05	0.61	0.228	0.97	2.1	0.08	0.008	1.61	75.82	99.57	0.83
DD1	79.67	0.69	10.12	2.77	0.02	0.65	0.411	1.19	2.14	0.12	0.028	1.67	73.01	99.48	1.17
DD1B	79.27	0.72	10.31	2.72	0.02	0.7	0.505	1.27	2.06	0.09	0.015	1.76	72.89	99.43	1.34
SF4	72.82	0.63	12.37	6.27	0.08	1.28	0.692	0.07	2.14	0.05	0.008	3.13	80.99	99.53	1.14
DD2	71.85	0.39	11.56	3.05	0.12	0.76	3.41	1.72	3.01	0.07	0.011	3.86	58.68	99.76	1.22

*CIA (chemical index of alteration), LOI (loss on ignition)

The origins of the sandstones are determined through the use of theoretical sandstone provenance fields developed by Dickinson (1985) in conjunction with the Q-F-L ternary diagram illustrated in Figure 29A. Upon analysis, it is evident from the modal Q-F-L ternary diagram that all fourteen samples of sandstone exhibit a composition indicative of a recycled orogenic source, as shown in Figure 29B. In addition to determining provenance, the sandstones are also classified using the Q-F-L ternary diagram adopted from Folk (1980), which places the samples within the sublitharenites category.
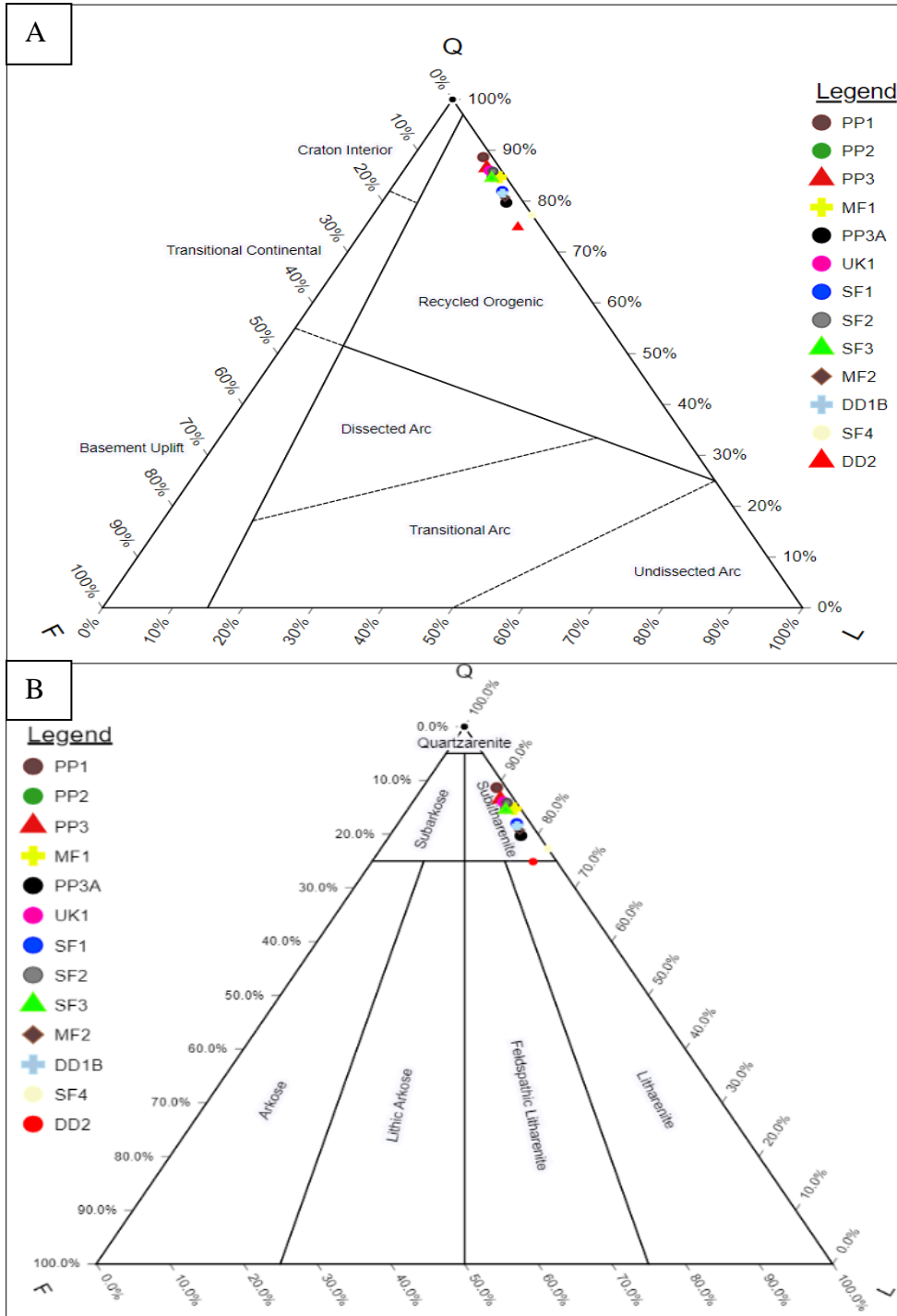
Figure 29. (A) Sandstone samples on ternary diagram for sandstone composition plot within sublitharenite (after Folk 1980). (B) Shows sandstone composition plot within recycled orogenic (after Dickinson, 1985). Q-F-L (quartz, feldspar, lithic fragments).

5.4 Scanning Electron Microscope (SEM)

The sandstone and coal samples underwent thorough examination using scanning electron microscopy (SEM) and energy dispersive X-ray (EDX) techniques. Table 4 provides a comprehensive list of the accessory minerals that were identified within the sandstone samples. While quartz remained the dominant mineral in both petrographic and mineral dominant map analyses, SEM-EDX analysis unveiled the presence of several heavy minerals including zircon, garnet, monazite, galena, and rutile within the sandstone samples. Furthermore, SEM-EDX analysis also revealed a diverse range of minerals such as silicates, carbonates, phosphates, oxides, sulfates, and sulfides (as shown in Table 5). These findings provide valuable insights into the provenance and composition of the sandstone samples under investigation.

Minerals such as zircon, garnet, rutile, monazite, chromite, and ilmenite resist alteration, whereas minerals such as olivine, pyroxene, and feldspar can alter more rapidly. SEM-EDX analysis also revealed that potassium feldspar (K-feldspar) contains small amounts of sodium (Na) in a solid solution, possibly a sanidine variety, and frequently exhibits a perthite texture with albite exsolution lamellae.

The albite sometimes contains trace amounts of potassium (K) and calcium (Ca), indicating the potential presence of anorthoclase. Biotite was more abundant than muscovite in the samples and showed signs of alteration to chlorite.

Most chlorite present is iron-rich and is closely associated with biotite, which contains titanium (Ti) in a solid solution. The matrix mainly comprises fine-grained quartz, chlorite, biotite, and muscovite (UK1). These are most likely formed diagenetically through the alteration of detrital feldspars and rock fragments. Additionally, calcite cement is observed in some places, most prominently in Sample DD2.

Table 4. Accessory minerals as determined by the SEM-EDX on sandstone samples.

| Minerals identified in sandstone samples		Abbreviation in images
silicates	quartz	qz
	K-feldspar	kfs
	albite	ab
	chlorite	chl
	biotite	bio
	muscovite	ms
	garnet	grt
	kaolinite	ka
	zircon	zr
carbonate	calcite	ca
phosphates	apatite	ap
	monazite	mz
	xenotime	xt
	wavellite	wav
oxides	rutile	rt
	ilmenite	ilm
	chromite	chr
	spinel	-
sulfate	barite	ba
sulfides	pyrite	py
	sphalerite	sph
	galena	ga
	Co-Ni pyrite	-
	pyrrhotite	po
	chalcopyrite	-
	tetrahedrite	-
	Fe cobaltite	co
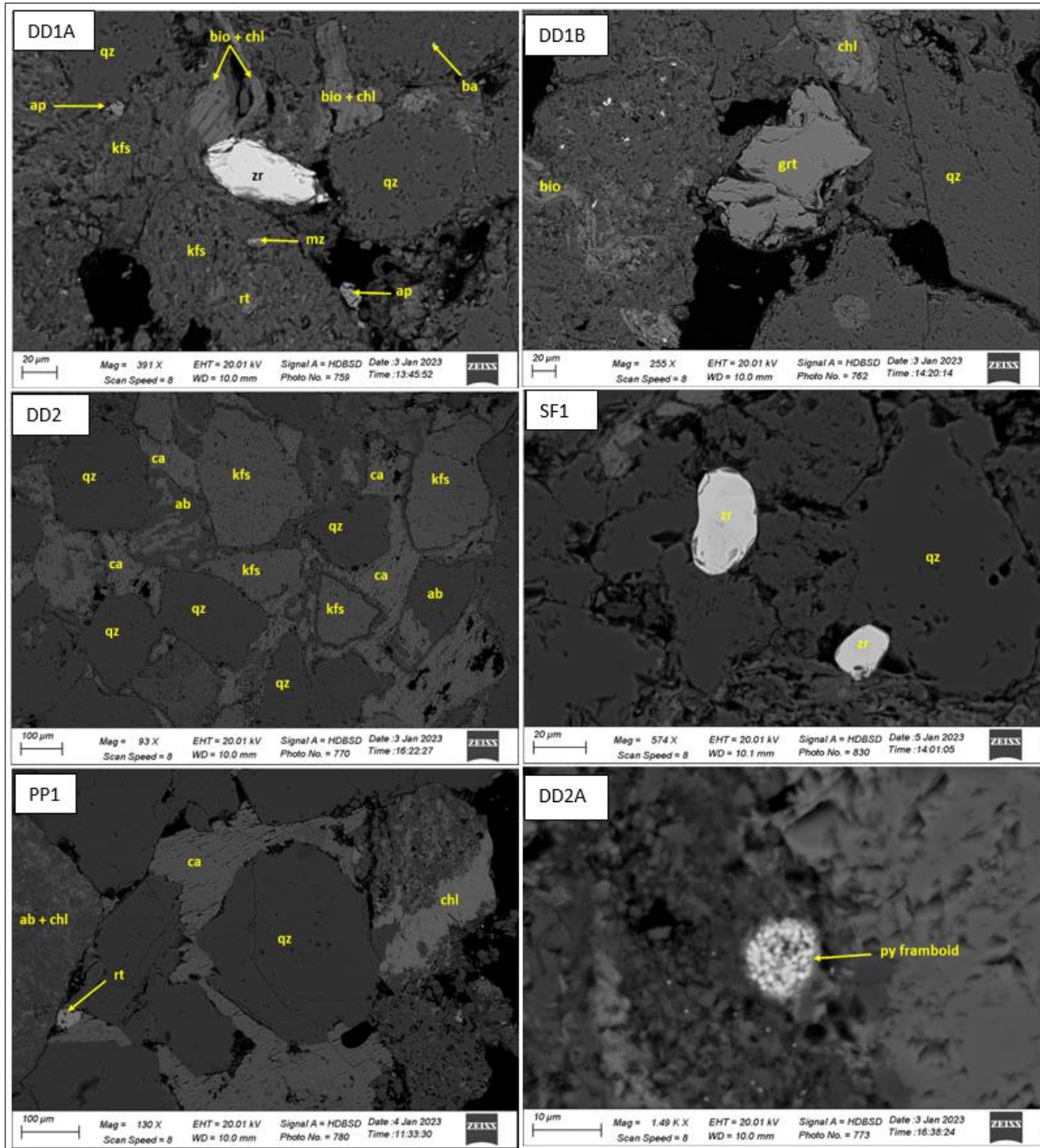
Figure 30. Back-scattered electron (BSE) images of the sandstone samples analysed. (DD1A) Chlorite, biotite, apatite k-feldspar, rutile, monazite, barite, quartz and zircon. (DD1B) Garnet, deformed biotite, chlorite and quartz. (DD2) Calcite, albite, k-feldspar and quartz. (SF1) sub-rounded detrital zircons with cracks on the edges. (PP1) Sub rounded quartz with calcite around it, chlorite and albite. (DD2A) Pyrite framboid.
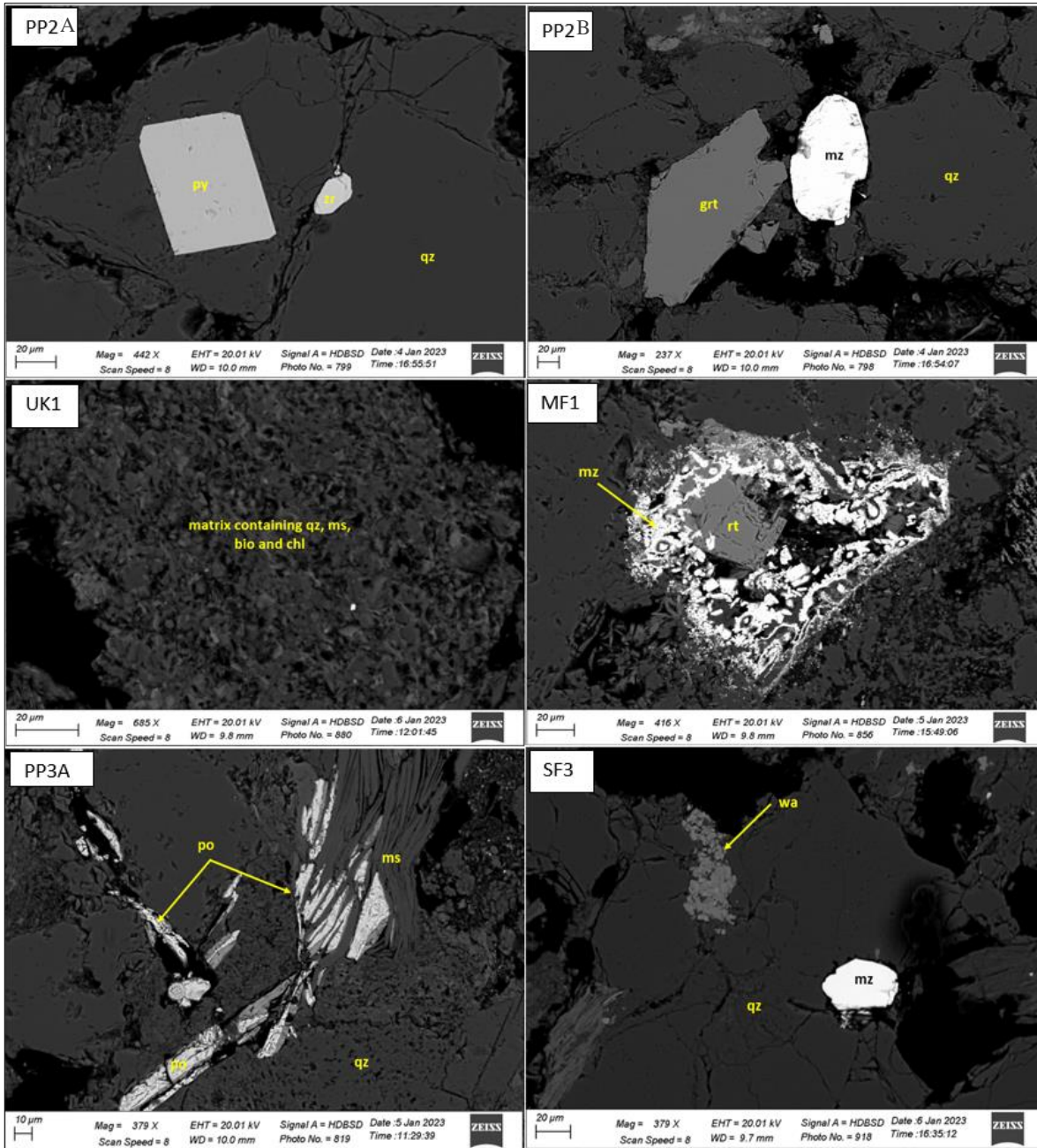
Figure 31. Back-scattered electron (BSE) images of the sandstone samples analysed. (PP2A) Pyrite, sub-rounded zircon and quartz. (PP2BB) garnet, monazite and quartz. (UK1) Matrix containing quartz, muscovite, chlorite and biotite. (MF1) rutile and monazite. (PP3A) Pyrrhotite, muscovite and quartz. (SF3) wavellite, monazite and quartz.

5.5 Concentration of Rare Earth Elements in coal

A set of 35 coal samples from the two main coal seams of the Bamboesberg Member (Guba and Indwe Seams) were assessed for their potential concentration of rare earth elements (REE). The samples were sourced from informal mining activities, abandoned mine sites, and exposed surface seams in the regions of Molteno, Skerkstroom, Dordrecht, Cala and Indwe (Figure 33). The primary objective of this chapter is to assess the concentration of REE and identify the minerals hosting these elements within the coal seams of the Bamboesberg Member.

REE constitutes a group of seventeen metallic elements in the periodic table, referred to as lanthanides, ranging from lanthanum (La) to lutetium (Lu), as depicted in Figure 32. In this study, we included scandium (Sc) and yttrium (Y) as part of the REE because they occur in the same ore sources as lanthanides and possess similar chemical properties (Walters et al., 2011), as defined by the International Union of Pure and Applied Chemistry (IUPAC) (Kolker et al., 2017). The names and symbols of these REE are provided in Table 5. Lanthanides are typically categorised as light rare earth elements (LREE), ranging from lanthanum to europium, and heavy rare earth elements (HREE), ranging from gadolinium to lutetium (Figure 32) (Walters et al., 2011). Based on atomic number distinctions, REE are classified as light (including Sc, La, Ce, Pr, Nd, Pm, Sm, Eu, and Gd) and heavy (encompassing Y, Tb, Dy, Ho, Er, Tm, Yb, and Lu) (Seredin and Dai, 2012; Lin et al., 2017).

Table 5. **Symbols and names of REE.**

Symbol	Name	Symbol	Name
La	lanthanum	Tb	terbium
Ce	cerium	Dy	dysprosium
Pr	praseodymium	Ho	holmium
Nd	neodymium	Er	erbium
Pm	promethium	Tm	thulium
Sm	samarium	Yb	ytterbium
Eu	europium	Lu	lutetium
Gd	gadolinium	Y	yttrium

Figure 32. Periodic table showing the rare earth elements including Sc and Y.

REE play a vital role in numerous industries, including petroleum refining, clean energy, automotive, electronics, and the military (Abaka-Wood et al., 2022; Fu et al., 2022). As a result, the growing demand for REE has spurred the exploration of alternative sources that could host these valuable metals. Traditionally, coal has been recognised for its significant contributions to the energy, chemical, and agricultural sectors. However, recent studies by Seredin et al., (2013), Zhang et al., (2015), Abaka-Wood et al., (2022), and Kolker et al., (2017) have revealed that coal also serves as a valuable alternative source of REE.

The concentration of REE in coal can be found in both the organic and inorganic phases (Fu et al., 2022; Kolker et al., 2017). Nonetheless, the concentration tends to be lower in the organic phase than in the inorganic phase. For instance, Fu et al., (2022) reported total REE concentrations in the organic and inorganic phases of coal to be 31 and 1,141 ppm, respectively. They found that the organic phase of feed coal contains 25% of the REE, whereas the inorganic phase comprises the remaining 75% (Fu et al., 2022).

Other studies (Gastaldo et al., 2013; Li et al., 2008; Yudovich et al., 2009; Seredin et al., 2013; Zhang et al., 2015) have indicated that the average REE concentrations in coal are 68 ppm for worldwide coals and 404 ppm for global coal ash. These findings underscore the potential of coal as a valuable source of REE.

The Inductively Coupled Plasma Mass Spectrometry (ICP-MS) was utilized to determine the occurrence and concentration of REE in the Bamboesberg coals. The ICP-MS results revealed the presence of both LREE and HREE. Most samples displayed a REE concentration ranging between 100 to 200 ppm, whereas five samples exhibited a higher concentration of over 350 ppm.
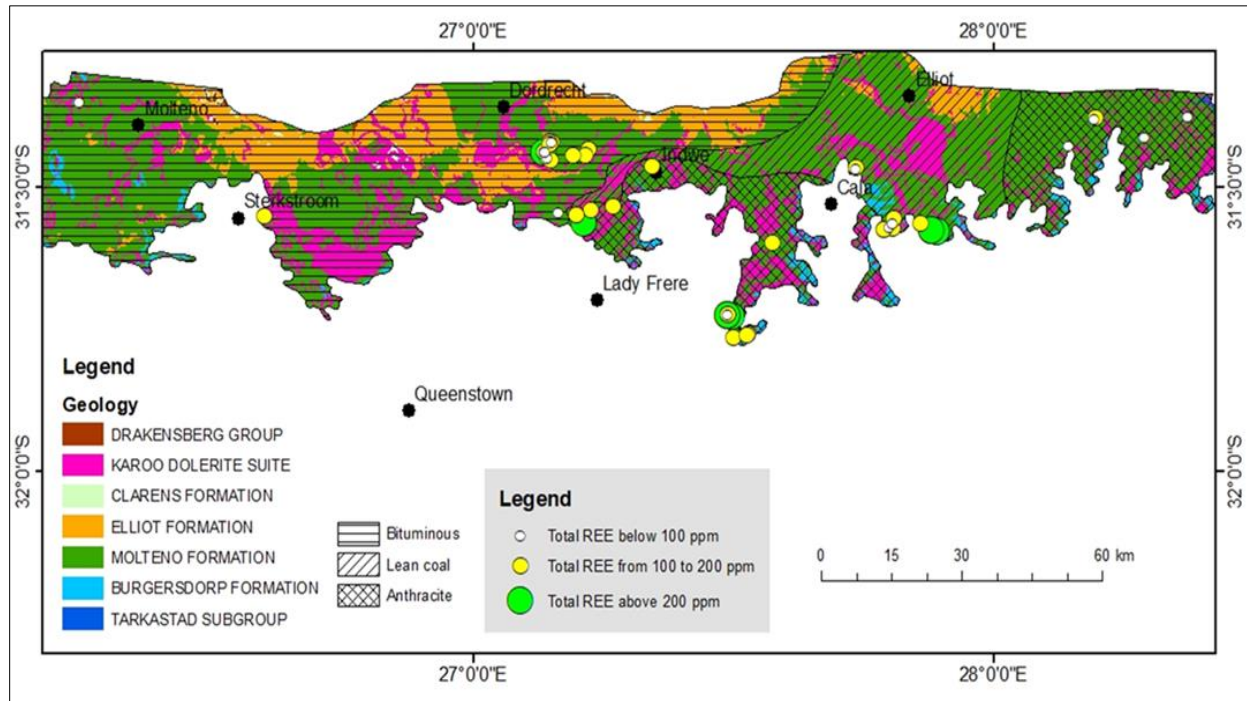

Figure 33. The location and concentration of samples that were analysed for REE in the Molteno-Indwe coalfield.

The SEM-EDX results on coal samples reveal the presence of monazite [(Ce,La,Nd,Th)PO4], parisite Ca(Ce,La) 2 (CO 3)3F 2, zircon [ZrSiO4] and xenotime [YPO4] (Figure 34). Monazite appears much more prevalent than xenotime, parisite, and zircon.
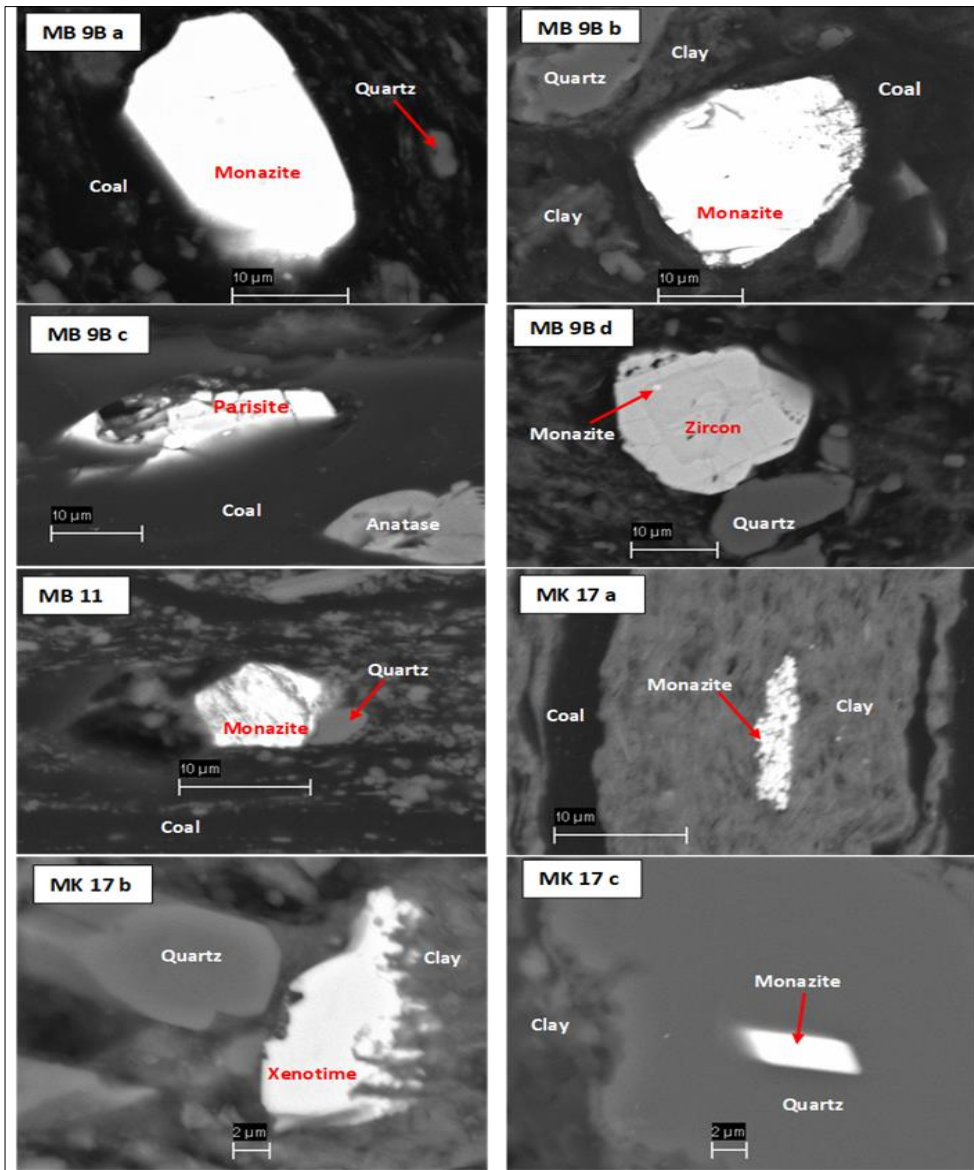

Figure 34. Back-scattered electron (BSE) images of the coal samples analysed showing the host REE bearing minerals. (MB98a, MB98bd, MB11, MK17a and MK17c) the images show the monazite. (MB 98c) the image shows parisite. (MB 98d) the image shows the zircon. (MK 17b) the image shows the xenotime.

5.6 Three-dimensional geological modelling

Geological features are three-dimensional (3-D). However, these features often appear on a two-dimensional surface, which may result in information loss or make understanding difficult. The virtual construction of three-dimensional (3-D) geological models is an emerging modern technology that is being used in numerous projects to predict and communicate the underlying geology (Turner and Gable, 2007; Wellmann and Caumon, 2018). These projects include regional geological characterisation, natural resource exploration, structural geology, geotechnical site characterisation, geophysics hydrology, and mining (Krajnovi et al., 2020).

In this study, the Leapfrog Geo™ software was used to model the geometrical distribution of the Bamboesberg Member within the Molteno-Indwe coalfield. Leapfrog Geo™ is a user-friendly tool, developed by SRK Consulting and Applied Research Association of New Zealand (ARANZ) (www.leapfrog3-D.com), for 3-D modelling and for the construction of boundary models that allows the development of conceptual models directly from boreholes, GIS, and other geological data without the need for laborious digitization. The main reason for creating a 3-D geological model of the Molteno Formation in the study area is to better understand the spatial and depth continuity of the Bamboesberg Member, which is the primary coal-hosting member. As a result, within the Molteno-Indwe coalfield, an area dominated by the Molteno Formation was selected for modelling. Dolerite intrusions were excluded from the modelling process because there are numerous dolerite dykes and sills in the area that make interpretation difficult and compromise the software's performance. The lithological and stratigraphical nomenclature of Bordy et al., (2005) was used to create the 3-D geological model of the Molteno Formation, i.e., the Bamboesberg and Indwe Members, and the Tsqima succession.

5.6.1 *Borehole data preparation*

Five boreholes (SF1/85, ZF1/85, BL1/85, PP5/65, and DD1/85) together with road cuts were selected for use in the regional 3-D modelling. Most of the boreholes in the study area have a shallow depth. Hence, only boreholes that exceed a depth of 100 m were selected. This depth selection is done to guarantee that the selected boreholes intersect the entire depth extent of the Molteno Formation. In addition, only boreholes with the full extent of lithological units from top to bottom were used. Spatially, boreholes were chosen to encompass the majority of the study area. Furthermore, four additional road cuts that cross-cut mountains, exposing most of the Molteno Formation lithologies, were complemented with the boreholes for modelling.

To represent surface features as accurately as possible, topographic data was obtained from the field using a Global Positioning System (GPS) and supplemented with Shuttle Radar Topographic Mission (SRTM) data to create a topographic layer used for 3-D geological modelling. The SRTM data was converted from raster to "point" shape files and saved as an Excel CSV file.
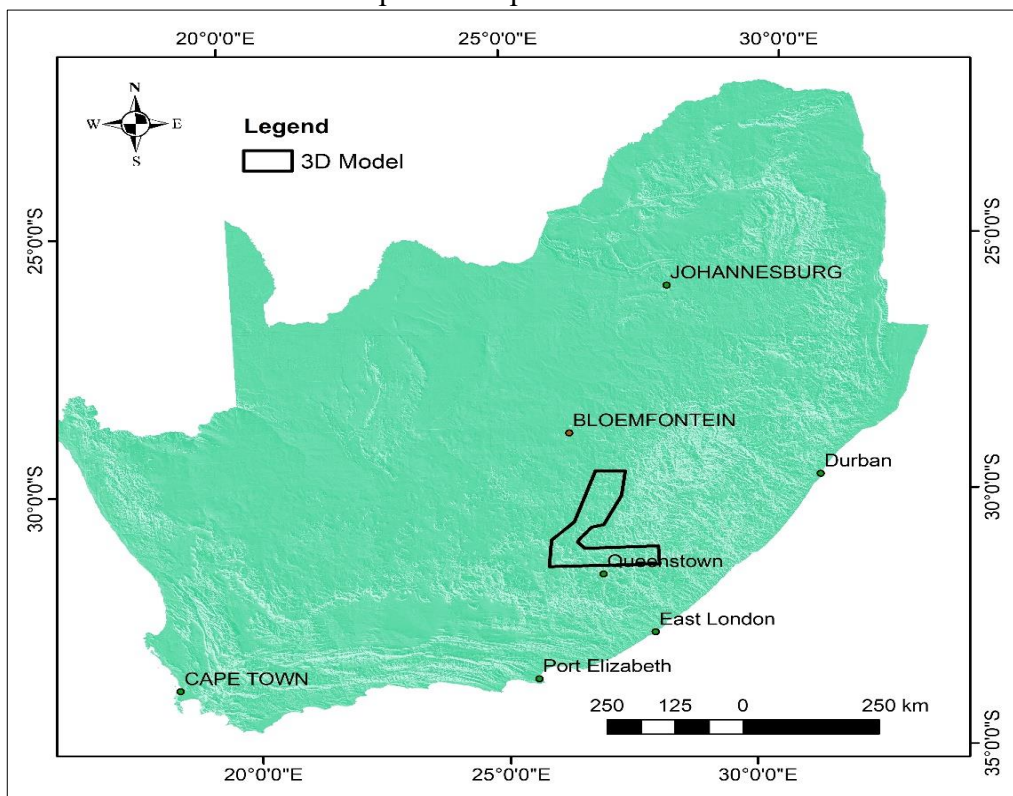

Figure 35. The extent of the 3D geological model.

5.6.2 Importing data

The five CSV files highlighted above (collar, lithology, assays, survey, and topographic files) were imported into Leapfrog Geo™. The errors due to import, depth contradictions, repeated intervals, etc. were corrected and rectified.

5.6.3 Geological modelling

The first step in 3-D geological modelling is to create a topographic layer that will serve as the limiting surface, allowing the 3-D geological model to begin only from the known actual surface on the ground. Other model constraints, such as depth extent (based on the depths of the drill holes) and the lateral extents, are then introduced into the process. Faults from the geological map are added into the modelling process, including their orientations.

A radial basis function was used to apply scattered 3-D data points to a single mathematical function to create a 3-D geological model by interpolating coded drill holes (lithology) and GIS data (structural data). The borehole data was used as the basis for determining the lithological, chronological, or stratigraphic sequence of the study area.

6 Discussion

6.1 Paleoclimate and paleoenvironment

The impact of weathering processes on sedimentary rock compositions can be evaluated in terms of the molecular percentage of the four major oxides (Al_2O_3, Na_2O, CaO and K_2O). The chemical index of alteration (CIA) has become a general guide to the degree of weathering in the provenance regions (Nesbit and Young, 1982). According to Oghenekome et al. (2018), high CIA values reflect increasing proportions of clay minerals with respect to feldspar, which can lead to an increased proportion of Al_2O_3 in kaolinite. The CIA value not only serves as an indicator of the chemical weathering of detritus in the source rock but also offers valuable insights into the prevailing climatic conditions during the sedimentary rock formation process. This parameter, as highlighted by Madukwe et al. (2014) and Oghenekome et al. (2018), provides a useful estimate for understanding past environmental conditions. Generally, fresh igneous rocks or unweathered upper crust have CIA values of approximately 50, but extensively weathered rocks have values approaching 100.

The CIA index of the Bamboesberg sandstones was calculated using the formula of Nesbit and Young (1982).

$$CIA = [Al_2O_3/ (Al_2O_3+CaO^* + Na_2O + K_2O)]\ 100.$$

When the CaO molar content is less than that of Na_2O, the measured CaO content can be used for CaO^*. The CIA value ranges from 58.88 to 80.99%, as shown in Table 3, with an overall average of 72.80% for the sandstones. Sample DD2 has a low CIA value compared with other samples, implying that it has been less weathered in comparison with others. The CIA index of these sandstones indicates that these sediments originated as a result of moderate weathering from the source.
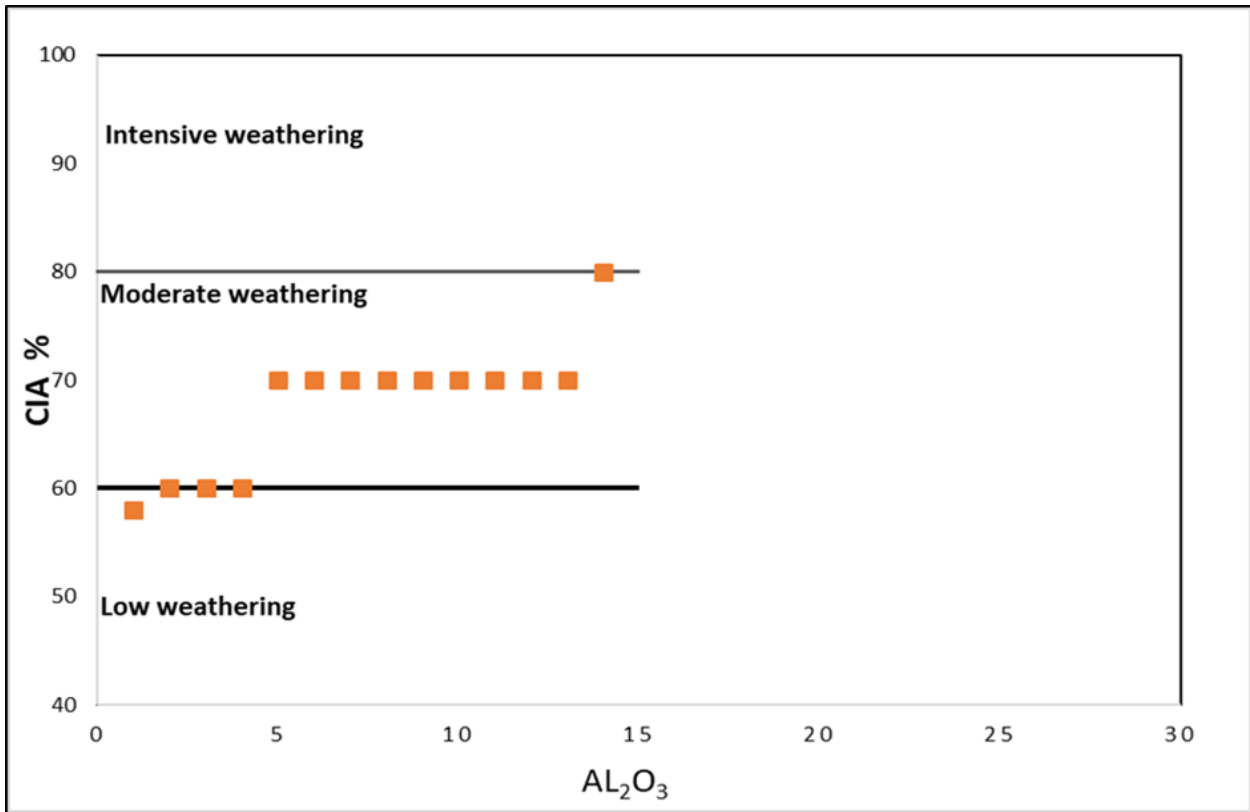
Figure 36. Plot showing most of the samples from the sandstones results of moderate weathering.

The sandstones of the Bamboesberg Member typically exhibit a coarse to medium-grained texture, transitioning into fine grains in the form of siltstone or carbonaceous mudstone. These sandstone units are characterized by four distinct facies - (Sp), (Sh), (Sr), and (Sm), These facies are associated with the network of fluvial systems, deposited in arid to semi-arid landscape. Quartz, being the predominant mineral, is composed of monocrystalline grains that display poor sorting and sub-angular to sub-rounded shapes. The abundance of monocrystalline quartz grains in the sedimentary rock suggests that it originated from a previously eroded source. Monocrystalline quartz grains originate from plutonic, hydrothermal, and recycled sedimentary sources, while polycrystalline quartz grains are recrystallized and stretched metamorphic types (Baiyegunhi et al., 2017). The presence of monocrystalline quartz grains indicates that the sediments were mostly produced from granitic sources. The presence of silica cement, which is common in the sandstones, could have resulted from the alteration of feldspar and the abrasion of quartz particles during transportation. Alternatively, it may have formed through pressure solution during later stages of diagenesis. Additionally, carbonate cement, particularly in the form of calcite ($CaCO_3$), is also found in these sandstones. This calcite cement is likely to have precipitated from the dissolution

of shelly material within the sediments. Moreover, it tends to fill the spaces between the individual grains, contributing to the overall matrix material which mainly consists of fine-grained quartz, chlorite, biotite, and muscovite. According to the provenance analysis, the sandstones were probably derived from older sedimentary formations such as the Ecca and Dwyka Groups and are classified as sublitharenites. The presence of zircon, garnet, rutile, monazite, and chromite indicates silica-rich granitic and/or gneissic terrains. These silica-rich granitic and gneissic terrains may be the original sources of the Bamboesberg sandstones. The granitic materials might be from the cape granite while the gneissic materials from the Namaqua-Natal Metamorphic Province.

The Bamboesberg Member is distinguished by facies indicative of network fluvial systems, with its coal seams representing peat swamp formations associated with these systems, which are linked to high water levels (Christie, 1981; Cairncross et al., 1995) and slow, consistent rates of accommodation space creation. The Molteno Formation was part of a greater inland basin, which was bordered by the Gondwana mountain range in the south (Turner, 1983). Turner (1977, 1978) highlighted that Molteno Formation was deposited by two major flow systems directed towards the north-west and north-east, combining to form a single northward route leading to the floodplain.

The southern section of the Bamboesberg Member, which is posited to be its deepest part, exhibits a significant accumulation of sediments and the formation of comparatively thicker coal seams, as previously mentioned. This notable thickness terrestrial sediments and coal seams in the southern part can be attributed to the presence of more favourable conditions for sediment depositions and coal preservation. A key factor in this context is the existence of deeper accommodation space in the southern part of the basin, leading to a more substantial accumulation of sediments. The deeper accommodation space in this area could be linked to the proximity of the northern boundary of the southern conductive zone that is postulated to extend deep into the Namaqua-Natal Metamorphic Province (Hancox 2022, pers. comm.). In contrast, the northern part of the Bamboesberg Member, proximal to the Kaapvaal Craton – representing the southern boundary – presents a different scenario. The flexuring in the northern region (Kaapvaal Craton) is considerably more challenging as compared to the Namaqua-Natal Metamorphic Province in the south. As a geological entity that is both ancient and, consequently, thick and cold, the Kaapvaal Craton renders the creation of accommodation space in the north substantially more difficult, as compared to the hot and younger Namaqua-Natal Metamorphic Province in the south (Hancox and Rubidge 2022, pers. comm.). This stark contrast between the southern and northern sections of the Bamboesberg Member basin may have played a crucial role in the distribution and characteristics of coal seam formation within the region.

6.2   Potential for Rare Earth Elements

This section aims to understand the concentration of rare earth elements on coal samples collected from the Bamboesberg Member. The ICP-MS analysis of the coal samples from the Bamboesberg Member revealed the presence of both LREE (La, Ce, Pr, Nd, Pm, Sm and Eu) and HREE (Gd, Tb, Dy, Ho, Er, Tm, Yb). La is the most prevalent element in most coal samples, followed by Sm, Eu, Dy, and Yb.

Majority of the coal samples have a total REE between 100 and 200 ppm, while five samples have a total REE above 350 ppm. Roth et al. (2017) undertook a comprehensive investigation into the possibility of extracting rare earth elements (REE) from fly ash, a byproduct of coal combustion. The study focused on fly ash sourced from Ohio, USA, which exhibited a total REE content of 358 ppm. In a separate study conducted by Yang et al. (2019), researchers examined the leaching potential of REE from coal sources in the Illinois Basin, USA. The coal samples analysed by Yang et al. (2019) displayed varying total REE concentrations ranging from 84 to 929 ppm, with the majority falling within the range of 190 to 404 ppm.

The average concentration of REE in worldwide coal has been reported to be 68 ppm, whereas in global coal ash, the concentration increases to 404 ppm (Seredin et al., 2012). Thus, the REE concentration of the Bamboesberg Member coal is on par with the established. The Bamboesberg coal sample concentrations were normalized to chondrite and the Upper Continental Crust values.
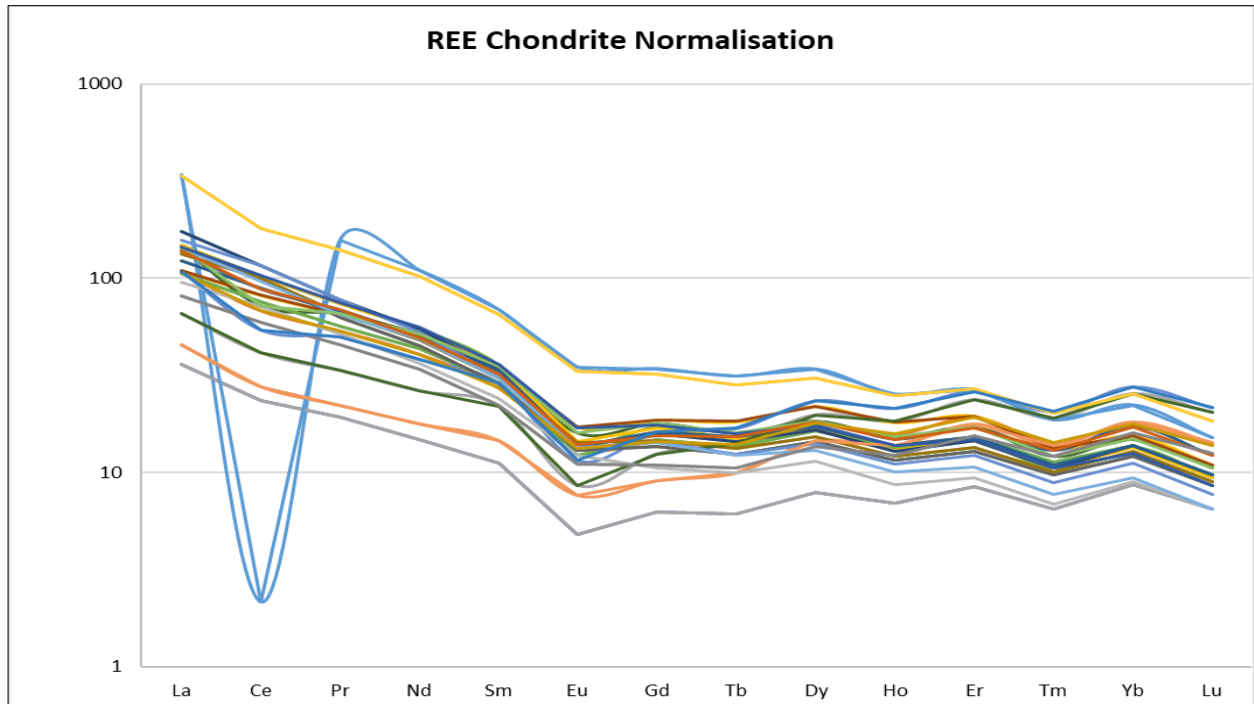
Figure 37. Chondrite-normalized REE distribution patterns for Bamboesberg coals (Taylor and McLennan, 1985).
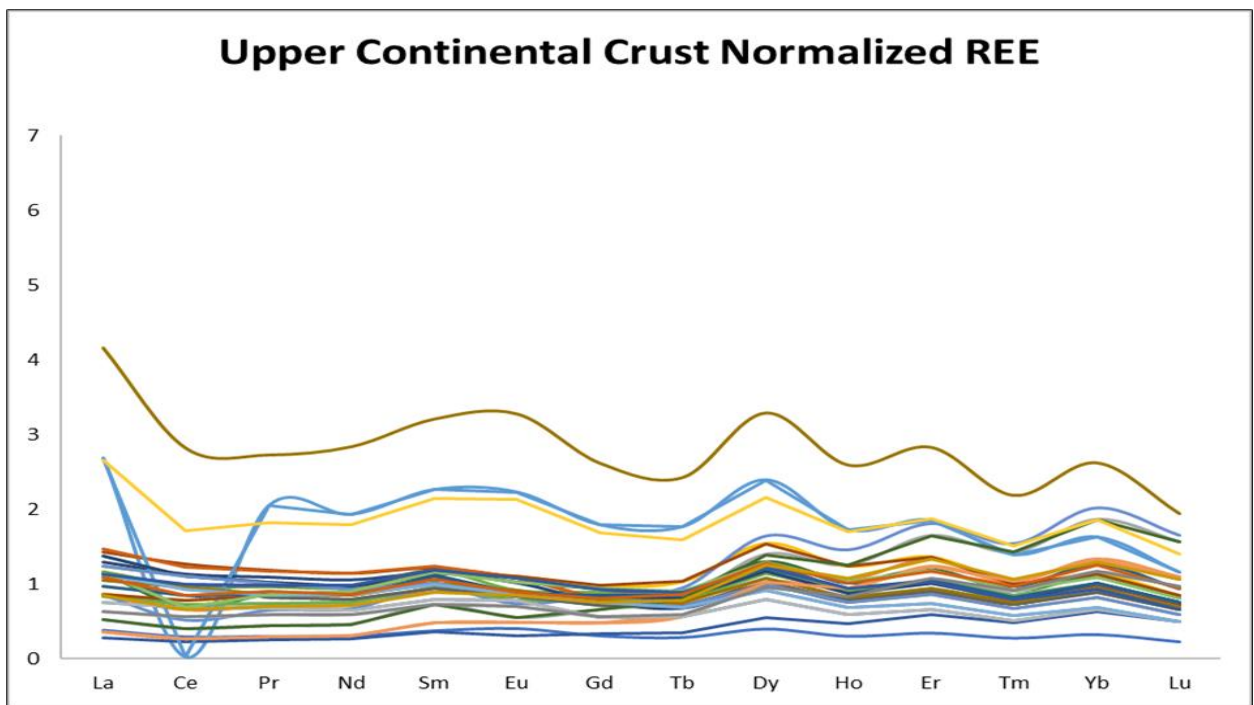

Figure 38. Upper continental crust normalization REE distribution patterns of Bamboesberg coals (Taylor and McLennan, 1985).

The chondrite normalized REE plot for the Bamboesberg coal samples (Figure 37) illustrates a notable disparity in the distribution of rare earth elements similar to the Chinese (Luzhou coalfield) and US coals studied by Kolker et al. (2017) and Dai et al. (2008), respectively. It is evident that this specific coal source exhibits a significant enrichment in light rare earth elements compared to heavy rare earth elements. The upper continental crust normalization (Figure 38) shows the horizontal pattern with negative Eu anomalies in most samples.

The cut-off grade for extracting rare earths from coal is 130 ppm (Fu et al., 2022). In the realm of REE found within coal, the application of a cut-off grade of 130 ppm (parts per million) implies that solely coal deposits containing REE concentrations of 130 ppm or greater would be deemed suitable for extraction.

Once the coal is combusted or burnt, the REE content in the resulting fly ash and bottom ash becomes concentrated, leading to an overall increase in the total REE present in the ash. In order to economically extract the REE from coal, it is necessary for the coal to undergo combustion for electricity generation. Additionally, a comprehensive study on the enrichment factor of REE in the remaining ash should be carried out to further understand its potential for extraction.

The SEM-EDS examination of Bamboesberg coal samples indicates the presence REE bearing minerals such as monazite parisite zircon and xenotime. The SEM-EDS also revealed the presence of quartz, anatase and clay minerals in the coal samples. Detrital monazite grains were observed to be rounded and anhedral, while detrital zircon grains appeared to be sub-rounded to round. The detrital grains of xenotime and parisite are subhedral. Occasionally, monazite was found as an inclusion within zircon, as depicted in Figure 34MB9bd.

According to various studies (Lin et al., 2017; Wu et al., 2022), concentrations of REE are present in both organic and inorganic matter in coal. According to the findings of this study, a certain concentration of REE, most likely a high concentration, is associated with inorganic matter in Bamboesberg Member coals. However, more research is needed to completely explain the prevalence of REE in the organic phase.
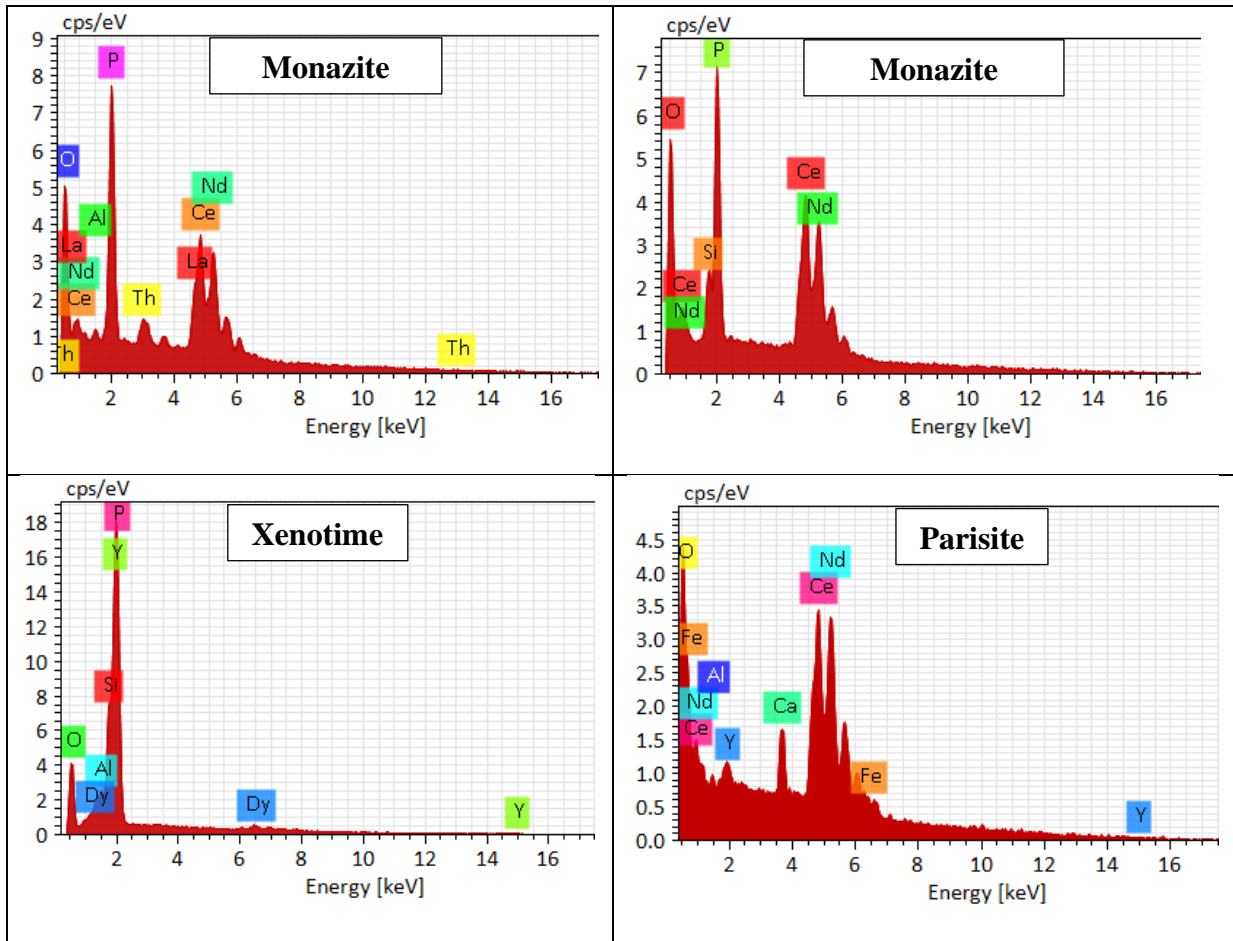
Figure 39. EDX spectrum showing rare earth hosting minerals composition.

The matrix correlation results show a good correlation between REE and Y of approximately 77%. Y is strongly correlated with HREE elements, particularly Dy, Er, Tm, Lu, and Ho (Figure 40). Ce, Pr, Nd, La, and Eu are the LREE that significantly correlate with Y. Both LREE and HREE show poor correlations with U, Th, volatiles, ash, and CV (Figure 40). The LREE that strongly correlate with Y are Ce, Pr, Nd, La, and Eu. Both LREE and HREE showed poor correlations with U, Th, volatiles, ash and calorific values (CV) (Figure 40). There is a negative correlation between ash content and CV. In addition, Yb shows a weak correlation with La, Ce, Pr and Nd.
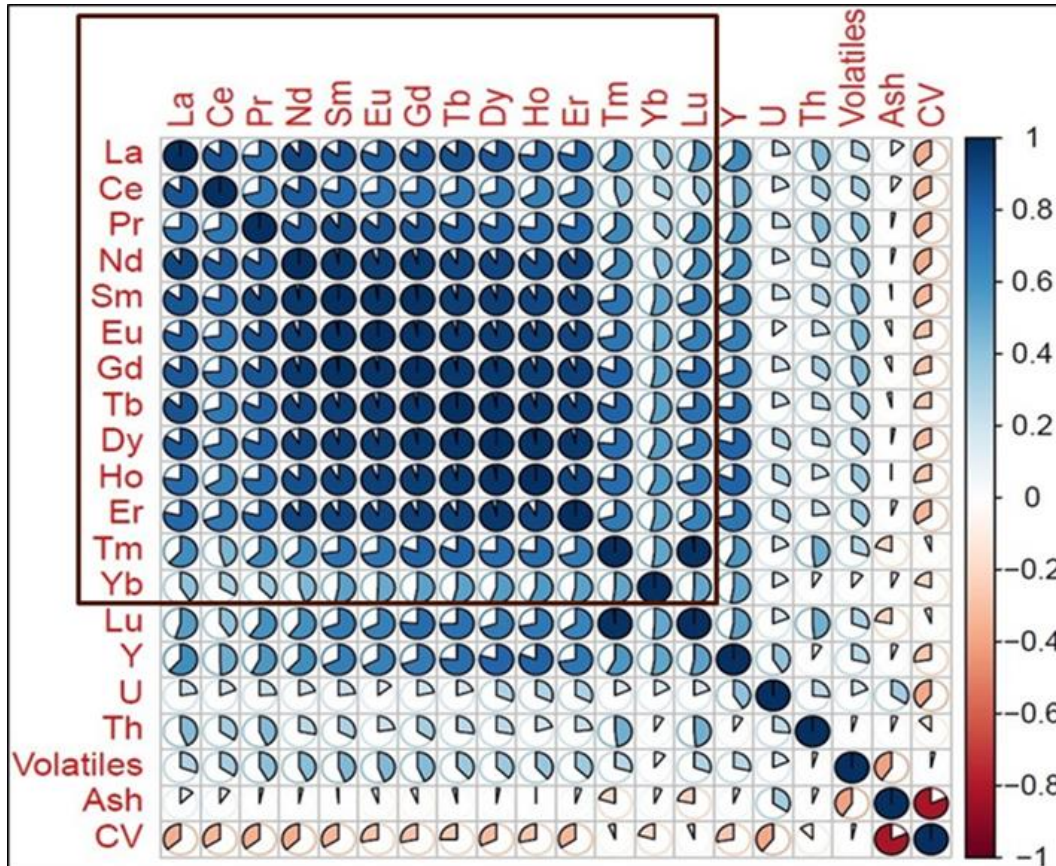
Figure 40. Matrix correlation coefficients represented by a colour scale. White represents a correlation coefficient of zero, while darker blues represent stronger positive correlations, and darker reds represent stronger negative correlations.

6.3 Interpretation of Geological modelling

The model illustrates that the geometry of the sedimentary sequence of the Bamboesberg Member is wedged between the Beaufort Group and the Indwe Member (Figure 41). The Indwe Member and Tsqima succession are less common in the western and central coalfields. The Bamboesberg Member is more exposed in the western (Molteno) and central (Indwe) sections of the coalfield. Consequently, these parts of the coalfield are the sweet spots for coal prospecting (Guba and Indwe seams), since the coal seams are less deep and covered by fewer members of the Molteno Formation than the eastern portion of the coalfield. The absence or scarcity of upper Molteno Formation members in the west and central parts could be explained by erosion or non-deposition. Five sandstone cycles are more prominent in the southern part of the coalfield (Figure 42), while the west and the northern part of the coalfield comprise fewer sandstone cycles. This indicates that the occurrence coal seams specifically, the laterally persistent Guba and Indwe seams) further west and north (north of Zastron) is very low.
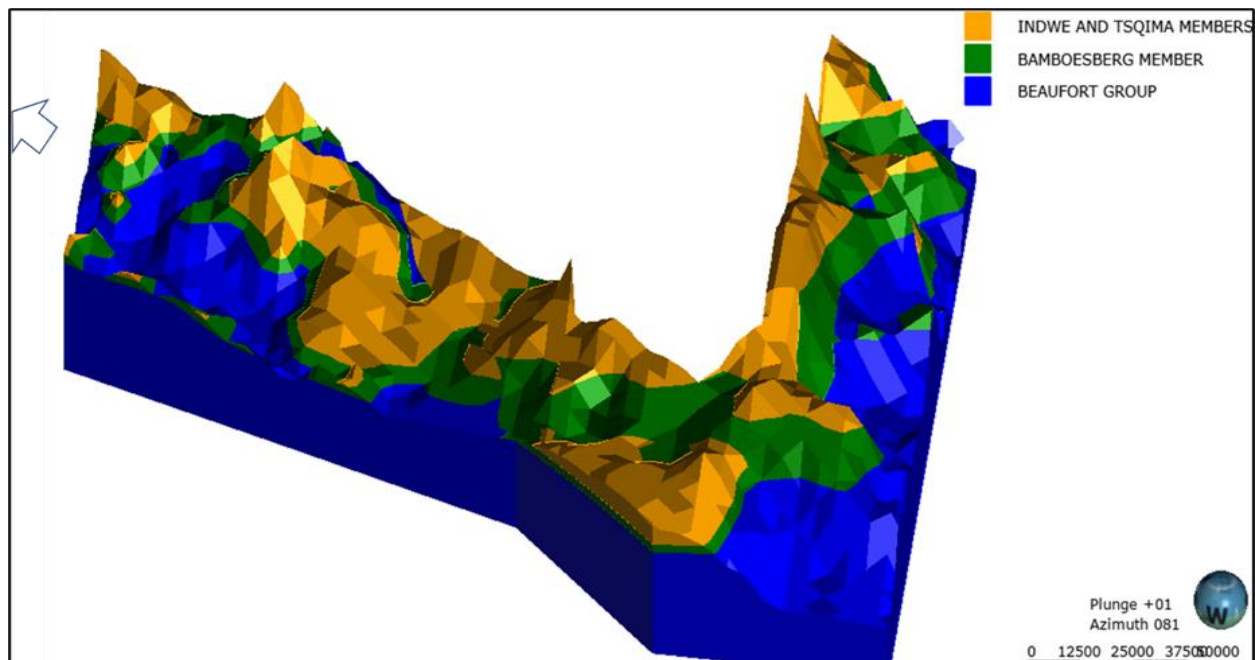

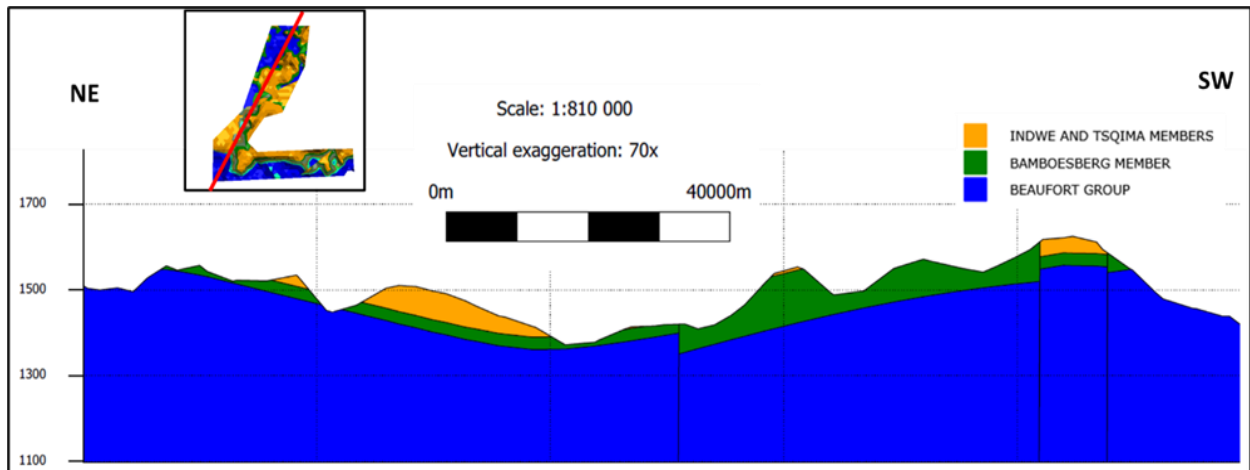**Figure 41.3D geological model looking north-eastwards. Vertical exaggeration 70.**

Figure 42. NE-SW section of the 3D geological model. The vertical exaggeration is set at 70.
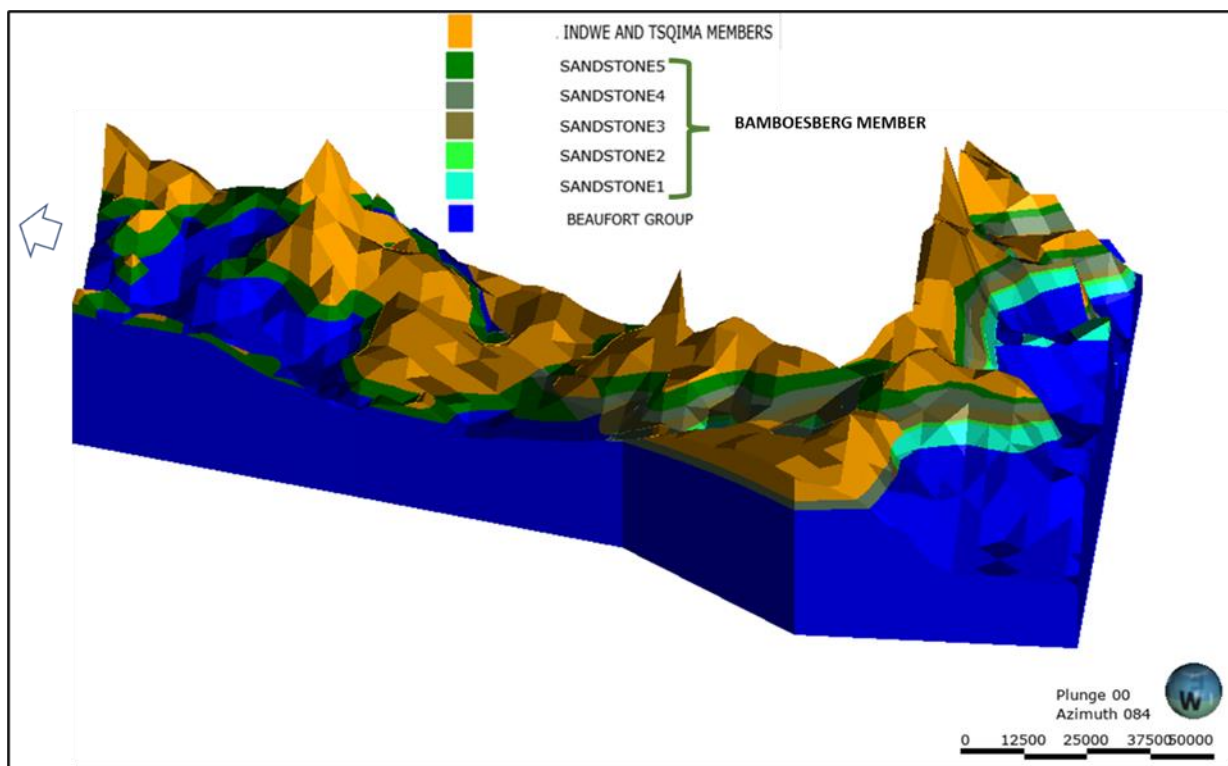

Figure 43. 3D geological model looking northwards. Vertical exaggeration is set at 70.

The Bamboesberg Member attains its maximum thickness of ~200 m in the south and then abruptly disappears in the far western part of the coalfield (Hofmeyr and Steynsburg). The geometry of the Bamboesberg Member exhibits a concave shape in the centre of the coalfield (around Indwe and Guba area), with a thickness of up to 120 m towards the centre and pinches out by up to 20 m in the north (Figure 44). Even though the thickest part of the Bamboesberg Member is on the western side of the study area, around Bushmanhoek Pass, where it attains a thickness of about 200 m, the eastern side of the model (at around Cala Pass) reveals that the geometry of the Bamboesberg Member deepens and still shows a thickness of ~160 m.

It is, therefore, feasible that the potential for coal seams (i.e., Guba and Indwe seams) east of the Cala Pass is good. Further coal exploration should therefore focus on the less well-known eastern side of the Molteno-Indwe coalfield. The Indwe Member and Tsqima succession are more prominent in the coalfield's eastern part. This is consistent with Christie (1981) and could imply that the upper coal seams (i.e., Molteno and Gubenxa) are present because they are linked with the upper stratigraphy of the Molteno Formation.
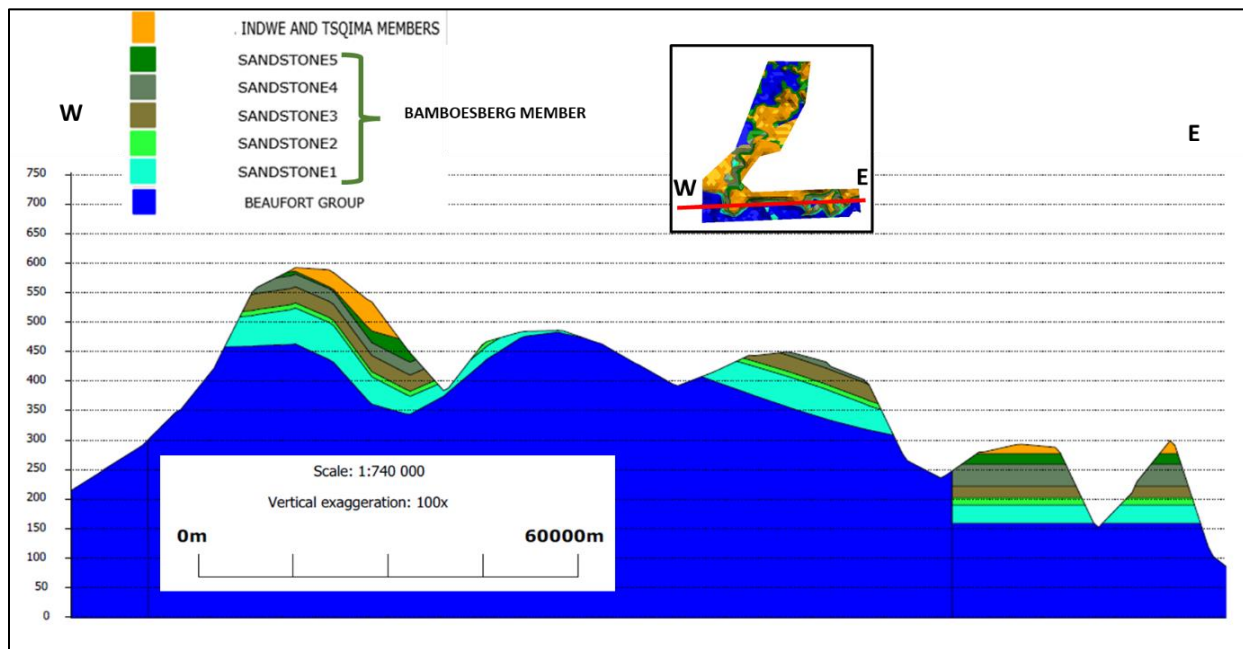

Figure 44. W-E section of the 3D geological model. The vertical exaggeration is set at 100.

7 CONCLUSIONS AND RECOMMENDATIONS

7.1 Conclusions

In this study, a variety of datasets have been meticulously analysed to gain insights into the characteristics of the Bamboesberg Member sandstones within the Molteno-Indwe coalfield. The research utilised an array of techniques, including borehole logging, facies descriptions, mineral and elementary composition, to provide a detailed characterization of these sandstones.

Based on the results of this study, the Bamboesberg sandstone cycles were deposited in semi-arid climate conditions by network fluvial systems and undergo moderate weathering from the original source. The study also revealed that these sandstones are derived from silica-rich granitic sources and gneissic terrain. In addition to showing characteristics of recycled orogenic sources, these sandstones are classified as sublitharenites.

The ICP-MS analysis reveal that most of the coal samples from the Bamboesberg Member have a concentration above the cut-off grade for extracting rare earths from coal is 130 ppm. The Upper continental crust-normalization of rare earth elements from the Bamboesberg coal samples reveal similar patterns, to those from other coalfields such as Luzhou coalfield in China. REE-bearing minerals (monazite, parisite, zircon, and xenotime) are known to host REE identified in coal samples by the SEM-EDX.

The 3D geological model of the Bamboesberg Member provides valuable insights into the geographical distribution of this Member within the coalfield. This member known to host two most economically coal seams (Guba and Indwe) form a concave shape towards the centre of the coalfield. The Member is generally less covered in the western (Molteno) and the central (Indwe) parts of the coalfield - overlaid by Indwe Member only. These parts of the coalfields become the sweet spots for coal prospecting of Guba and Indwe Seams, as the coal seams are not as deep.

7.2 Recommendations

Appropriate ground geophysical surveys, such as magnetics, magnetotellurics, 2D seismic, and resistivity should be conducted to better understand basement variations and structures and for eventual drill hole siting and planning in this region. This would allow one to examine the presence and continuity of the coal seams and assess their quality, which is vital for determining the feasibility of coal production in the area.

This study provides crucial insights that not only enhance our understanding of the geological and mineralogical characteristics of the Bamboesberg Member, but also pave the way for future research, exploration, and economic exploitation of its resources.

However, to gain a more complete understanding of the source rock, further studies such as Laser Ablation zircon and garnet dating should be conducted.

References

Abaka-Wood, G.B., Addai-Mensah, J., Skinner, W. (2002). The concentration of rare earth elements from coal fly ash. Journal of the Southern African Institute of Mining and Metallurgy.

Al-Harbi OA, Khan M (2008) Provenance, diagenesis, tectonic setting and geochemistry of Tawil sandstone (Lower Devonian) in Central Saudi Arabia. J Asian Earth Sci 33:278–287 Journal of the Southern African Institute of Mining and Metallurgy, Volume. 122, No. 1, pp. 21-28.

Anderson, J.M. & Anderson, H.M. (1983). Palaeoflora of Southern Africa Molteno Formation (Triassic). Volume 1. Part 1. Introduction; Part 2. Dicroidium. Balkema, Rotterdam.

Anderson, J.M. & Anderson, H.M. (1989). Palaeoflora of Southern Africa Molteno Formation (Triassic). Volume 2. Gymnosperms (excluding Dicroidium). Balkema, Rotterdam.

Anderson, J.M. & Anderson, H.M. (1993a). Terrestrial flora and fauna of the Gondwana Triassic: Part 1—occurrences. In: Lucas, S.G. & Morales, M. (eds) The Non-marine Triassic. New Mexico Museum of Natural History and Science Bulletin, 3, pp. 3–12.

Anderson, J.M., Anderson, H.M. and Cruickshank, A.R.I. (1998) Late Triassic ecosystems of the Molteno /Lower Elliot biome of southern Africa. Palaeontology, Volume, 41.part 3, pp. 387-421.

Ashton, K., Wendy Z., and Marte, G. (2020). Uncertainty assessment for 3D geologic modeling of fault zones based on geologic inputs and prior knowledge. Solid Earth, 11, pp. 1457–1474. https://doi.org/10.5194/se-11-1457-2020.

Baiyegunhi, C. (2015). Geological and geophysical investigation of the southeastern Karoo Basin Unpublished MSc, University of Fort Hare, South Africa, pp. 1–294.

Baiyegunhi, C., Liu, K. and Gwavava, O. (2017). Diagenesis and reservoir properties of the Permian Ecca Group sandstones and mudrocks in the Eastern Cape Province, South Africa. Minerals, Volume 7, Issue 6.

Bamford, M. K. (2004). Diversity of the woody vegetation of Gondwana, Southern Africa. Gondwana Research,7, 1, pp. 153-164.

Bangert, B., Stollhofen, H., Lorenz, V. and Armstrong, R. (1999). The geochronology and significance of ash-fall tuffs in the glaciogenic Carboniferous-Permian Dwyka Group of Namibia and South Africa. Journal of African Earth Sciences, pp. 33–49.

Boggs, S. (2001). Principles of sedimentology and stratigraphy. (4th edition). Upper Saddle River, New Jersey 07458: Pearson Prentice Hall.

Bordy, E.M. and Catuneanu, O. (2002). Sedimentology and paleontology of upper Karoo aeolian strata (Early Jurassic) in the Tuli Basin, South Africa. Journal of African Earth Sciences, 35(2), pp. 301–314. https://doi.org/10.1016/S0899-5362(02)00103-3.

Bordy, E.M., Hancox, P.J. and Rubidge, B.S. (2004). Provenance study of the Late Triassic - Early Jurassic Elliot Formation, main Karoo Basin, South Africa', South African Journal of Geology, 107(4), pp. 587–602. https://doi.org/10.2113/gssajg.107.4.587.

Bordy, E.M., Hancox, P.J. and Rubidge, B.S. (2005a). The contact of the Molteno and Elliot formations through the main Karoo Basin, South Africa: A second-order sequence boundary', South African Journal of Geology, 108(3), pp. 351–364.

Bordy, E.M., Hancox, P.J. and Rubidge, B.S. (2005b). The contact of the Molteno and Elliot formations through the main Karoo Basin, South Africa: A second-order sequence boundary. South African Journal of Geology, 108(3), pp. 351–364.

Bristow, C.S. and Best J. L. (1993). Braided rivers perspectives and problems. Geological Society Special Publication No. 75, pp. 1-11.

Cadle, A.B., Cairncross, B., Christie, A. D.M. and Roberts, D. L. (1993). The Karoo Basin of South Africa: type basin for the coal-bearing deposits of southern Africa. International Journal of Coal Geology, 23(1–4), pp. 117–157.

Cairncross, B., Anderson, J. M. and Anderson, H. M. (1995). Palaeoecology of the Triassic Molteno Formation, Karoo Basin, South Africa - sedimentological and palaeontological evidence. South African Journal of Geology. Volume 98, Issue 4, pp. 452-478.

Catuneanu, O., Hancox, P.J. and Rubidge, B.S. (1998). Reciprocal flexural behaviour and contrasting stratigraphy: a new basin development model for the Karoo retroarc foreland system, South Africa, Basin Research. Basin Research 10, pp. 417–439.

Catuneanu, O. and Elango, H.N. (2001). Tectonic control on fluvial styles: The Balfour formation of the Karoo Basin, South Africa. Sedimentary Geology, 140, (3–4), pp. 291–313.

Catuneanu, O., Hancox, P.J., Cairncross, B., Rubidge, B.S. (2002). Foredeep submarine fans and forebulge deltas: orogenic off-loading in the underfilled Karoo Basin. Journal of African Earth Sciences 35 (2002), pp. 301–314.

Catuneanu, O. (2004). Retroarc foreland systems-evolution through time. Journal of African Earth Sciences, 38(3), pp. 225–242. https://doi.org/10.1016/j.jafrearsci.2004.01.004.

Catuneanu, O., Wopfner, H., Eriksson, P.G., Cairncross, B., Rubidge, B. S. Smith, R.M.H., Hancox, P.J. (2005). The Karoo basins of south-central Africa. Journal of African Earth Sciences, 43(1–3), pp. 211–253.

Cobban, D.A., Rossouw, J.N., Versfeld K., Nel., D. (2009). Water quality considerations for opencast mining of the Molteno coal field, Indwe, Eastern Cape. International Mine Water.

Chima, P., Baiyegunhi, C., Liu, K., Gwavava, O. (2018). Diagenesis and rock properties of sandstones from the Stormberg Group, Karoo Supergroup in the Eastern Cape Province of South Africa. Journal of the Southern African Institute of Mining and Metallurgy.

Christie, A.D.M. (1988). Sedimentary Models for Coal Formation in the Klip River Coalfield. Unpublished PhD Thesis, University of Natal, pp. 46-182.

Coleman, J.M. (1969). The Brahmaputra River: Sedimentary Geology, pp. 129-239.

Cartesio, L.E.G. (2017). Processes and controls on shelf margin accretion and degradation: Karoo Basin, South Africa. Unpublished PhD thesis, University of Manchester, England, pp. 30-169.

Dickinson, W.R. (1985). Provenance Relations from Detrital Modes of Sandstones. In: G. G. Zuffa (Editor) Provenance of arenites. Dordrecht: D. Reidel, The Netherlands, pp. 333-361.

Eriksson, P.G. (1984). A Palaeoenvironmental analysis of the Molteno Formation in the Natal Drakensberg. Transkei. South African Journal of Geology, 87, pp. 237–244.

Fu, B., Howerb, J.C., Zhang, W., Luoa, G., Hua, H. and Yaoa, H. (2022). A review of rare earth elements and yttrium in coal ash: Content, modes of occurrences, combustion behaviour, and extraction methods. Progress in Energy and Combustion Science, 100954.

Gastaldo, R.A., Pludow, B.A. and Neveling, J. (2013). Mud aggregates from the Katberg Formation, South Africa: Additional evidence for Early Triassic degradational landscapes. Journal of Sedimentary Research, pp. 531–540. Available at: https://doi.org/10.2110/jsr.2013.45.

Hancox, P.J. (1998). A stratigraphical, sedimentological and paleoenvironmental synthesis of the Beaufort-Molteno contact, in the Karoo Basin, (1998). Unpublished PhD thesis, University of the Witwatersrand, pp. 404.

Hancox, P.J. and Götz, A.E. (2014). South Africa's coalfields - A 2014 perspective. International Journal of Coal Geology, 132, pp. 170–254.

Hancox, P.J. and Rubidge, B.S. (2023). The Beaufort-Stormberg Group contact – Implications for Karoo Basin development in the Triassic. Journal of African Earth Sciences 198 (2023) 104767.

Heinemann, M. and Buhmann, D. (1987). Coal-tonsteins from the Molteno Formation of the Maluti district. Transkei. South African Journal of Geology, 90 (3), pp. 296–304.

Herbert, C.T. and Compton, J.S. (2007). Depositional environments of the lower Permian Dwyka diamictite and Prince Albert shale inferred from the geochemistry of early diagenetic concretions, southwest Karoo Basin, South Africa, Sedimentary Geology, 194 (3–4), pp. 263–277.

Johnson, M. R., Van Vuuren C. J., Hegenberger W. F., Key, R., Show, U. (1996). Stratigraphy of the Karoo Supergroup in Southern Africa: an overview. Journal of African Earth Sciences, Volume, 23, No, pp. 3-15.

Kolker, A., Scott, C., Hower, J.C., Vazquez, J.A., Lopano, C.L., Dai, S. (2017). Distribution of rare earth elements in coal combustion fly ash, determined by SHRIMP–RG ion microprobe. International Journal of Coal Geology 184, pp. 1–10.

Koen, G.M. (1955). Heavy minerals as an aid to the correlation of sediments of the Karroo System in the northern part of the Union of South Africa, pp. 281-366

Lin, R., Howard, B.H., Roth, E.A., Bank, T.L., Granite, E.J., Soong, Y. (2017). Enrichment of rare earth elements from coal and coal by-products by physical separations. 34th Annual International Pittsburgh Coal Conference: Coal - Energy, Environment and Sustainable Development.

MacDonald, A.J. (1993). A reassessment of coal resources in the western part of the Molteno Coal Province. Bulletin Geological Survey South Africa. 116, p. 1-33.

Madukwe, H. Y., Akinmosin, A., Akinyemi, S. A., Adebayo, O. F., Aturamu, A. O., Ojo, A.O. (2015). Provenance, tectonic setting and maturity of the Ishara sandstone, South western, Nigeria: insight from major element geochemistry. Volume. 6, Issue, 12, pp. 11123-11133.

McKee, E.D., Crosby, E.J., and Berryhill, H.L. (1967). Flood deposits, Bijou Creek, Colorado, June 1965: Journal of Sedimentary Petrology, Volume. 87, pp. 829-851.

Melehan, S., Botziolis, CM., Angelos G., Catuneanu, O., Ruming, K., Holmes, E., Collins, W.J. (2021) Sedimentology and Stratigraphy of an Upper Permian Sedimentary Succession: Northern Sydney Basin, Southeastern Australia. Geosciences 2021, 11, 273.

Miall, A.D. (1977). A review of braided river stream depositional environment. Earth Science Reviews 13, pp. 1-62.

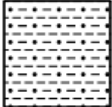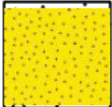Miall, A.D. (1996). The geology of fluvial deposits. Springer Berlin Heidelberg, Berlin, Germany.
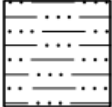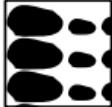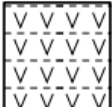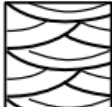
Miall, A.D. (1988). Architectural elements and bounding surfaces in fluvial deposits: anatomy of the Kayenta formation (lower Jurassic), Southwest Colorado. Sedimentary Geology, Volume. 55, pp. 233–262.

Nesbitt, H., Young, G. (1982). Early Proterozoic climates and plate motions inferred from major element chemistry of lutites. Nature, 299, pp. 715–717.

Nyathi, N. (2014). Stratigraphy, sedimentary facies and diagenesis of the Ecca Group, Karoo Supergroup in the Eastern Cape, South Africa. Unpublished MSc, University of Fort Hare, South Africa.

Oghenekome, M.E., Tapas K., Chatterjee, J.M., Donker, V.B., Napoleon, Q.H. (2018). Geochemistry and weathering history of the Balfour sandstone formation, Karoo basin, South Africa: Insight to provenance and tectonic setting. Journal of African Earth Sciences, 147, pp. 623–632.

Ore, H.T. (1963). Some criteria for recognition of braided stream deposits: University of Wyoming, Contributions to Geology, Volume. 3, pp. 1-14.

Phillips, C. (2014). Fluvial Facies Architecture and Provenance History of the Abrahamskraal-Teekloof Formation Transition (Lower Beaufort Group) in the Main Karoo Basin. Unpublished MSc thesis, University of Cape Town, South Africa.

Prévost, X. (2013). Review of the South African coal mining industry. 12 pp. https://cer.org.za/wp-content/uploads/2017/12/Annexure-P.pdf.

Reik, E.F. (1974). Upper Triassic insects from the Molteno Formation South Africa. Palaeontologia Africana, 17, pp. 19–31.

Reik, E.F. (1976). A new collection of insects from the Upper Triassic of South Africa. Annals ofthe Natal Museum, 22, pp. 791–820.

Reynolds, A.J. (1979). Geochemical and mineralogical aspects of the molteno formation, South Africa. Unpublished BSc (Hons), University of Rhodes, South Africa.

Rust (1962). Geology of the Molteno Stage. pp. 171-181.

SACS (South African Committee for Stratigraphy) (1980). Stratigraphy of South Africa. Part I (Compiler L.E. Kent), Lithostratigraphy of the Republic of South Africa, South West-Africa/Namibia, and the Republics of Bophuthatswana, Transkei, and Venda, Geological Survey South Africa Handbook. 8, pp. 690.

Scott, A.C., Anderson, J.M., Anderson, H.M. and Heidi M (2004). Evidence of plant-insect interactions in the Upper-Triassic Molteno Formation of South Africa. Journal of the Geological Society. Volume 61, Issue 3, pp. 401-410.

Seredin, V.V., Dai, S. (2012). Coal deposits as potential alternative sources for lanthanides and yttrium. International Journal of Coal Geology, 94, pp. 67–93.

Seredin, V.V., Dai, S., Sun, Y., Chekryzhov, I.Y. (2013). Coal deposits as promising sources of rare metals for alternative power and energy-efficient technologies. Applied Geochemistry, Volume. 31. pp. 1−11. http://dx.doi.org/10.1016/j.apgeochem.2013.01.009.

Setladi, M.C. (2023). A petrological investigation of the Guba Seam at Elitheni Colliery. Un published MSc thesis (Economic Geology) University of the Witwatersrand, South Africa.

Smith, N.D. (1970). The braided stream depositional environment: A comparison of the Platte River with some Silurian clastic rocks, north-central Appalachians. Geological Society of America Bulletin, Volume. 81, pp. 2993-3014.

Taylor, S.R. and McLennan, S.M. (1985). The Continental Crust: Its Composition and Evolution. Blackwell Scientific Publishers, pp. 312.

Terry, R. D. and Chilingar, C.V. (1955). Summary of Concerning some additional aids in studying sedimentary formations. Journal of Sedimentary Petrology, 25, pp.229-214.

Turner, A. and Gable, C. (2007). A review of geological modeling. Minnesota Geological Survey, St. Paul, Minnesota, USA.

Turner, B.R., (1971b). The geology and coal resources of the North-eastern Cape Province. Geological Survey of South Africa. 52, pp. 1–74.

Turner, B.R. (1975). The stratigraphy and sedimentary history of the Molteno Formation in the main Karoo Basin of South Africa and Lesotho. Unpublished PhD thesis, University of the Witwatersrand, South Africa, pp. 314.

Turner, B.R. (1977). Fluviatile cross-bedding patterns in the Upper Triassic Molteno Formation of the Karoo (Gondwana) Supergroup in South Africa and Lesotho. Transactions Geological Society of South Africa, 80, pp. 241-252.

Turner, B. (1981). Revised stratigraphy of the Beaufort Group in the southern Karoo Basin, 24, pp. 87–98.

Theron, J.C., (1970). Some Geological Aspects of the Beaufort Series in the OFS. Unpublished Ph.D. thesis, University of the Orange Free State, South Africa. pp. 244.

Uys, J. (2007). Lithostratigraphy, depositional environments and sedimentology of the Permian Vryheid Formation (Karoo Supergroup), Arnot North, Witbank Coalfield, South Africa. MSc thesis, University of Johannesburg, South Africa. pp. 117.

Veevers, J.J., Cole, D.I., Cowan, E.J. (1994). Southern Africa: Karoo Basin and Cape Fold Belt, Memoir of the Geological Society of America, 184(1), pp. 223–279. https://doi.org/10.1130/MEM184-p223.

Viglietti, P.A. (2016). Stratigraphy and sedimentary environments of the Late Permian {Dicynodon} Assemblage Zone (Karoo Supergroup, South Africa) and implications for basin development. PhD thesis, University of the Witwatersrand, South Africa.

Wellmann, F. and Caumon, G. (2018). 3-D Structural geological models: Concepts, methods and uncertainties. Advances in Geophysics, 59, Elsevier, pp. 1-121.

William, P.F., and Rust, B.R. (1969). The sedimentology of a braided river. Journal of Sedimentary Petrology, Volume. 39, pp. 649-679.

Wu, S., Haiying, Y., Haifeng, F., Yong, X., Qingtian, M., Shan, H., Xingxiang, G. (2022). Assessment of the Effect of Organic Matter on Rare Earth Elements and Yttrium Using the Zhijin Early Cambrian Phosphorite as an Example. Minerals 2022, 12, 876.

Yudovich, Y. and Ketris, M.P. (2009). Estimations of Clarkes for Carbonaceous Biolithes: World Averages for Trace Element Contents in Black Shales and Coals. International Journal of Coal Geology, 78, pp. 135-148. https://doi.org/10.1016/j.coal.2009.01.002.

Zhang, W., Groppo, J., Honaker, R. (2015). Ash beneficiation for REE recovery. 2015 World of Coal Ash (WOCA) Conference in Nasvhille, TN - May 5-7, 2015. pp. 11.

8 APPENDIX A.

Lithology legend for (Figure 13, 14 and 15)